# HUBBLE SPACE TELESCOPE/WFPC2 INVESTIGATION OF THE NUCLEAR MORPHOLOGY IN THE TOOMRE SEQUENCE OF MERGING GALAXIES[1]

SEPPO LAINE
SIRTF Science Center, Mail Code 220-6, California Institute of Technology, Pasadena, CA 91125
seppo@ipac.caltech.edu

ROELAND P. VAN DER MAREL, JÖRN ROSSA AND TORSTEN BÖKER[2]
Space Telescope Science Institute, 3700 San Martin Drive, Baltimore, MD 21218
marel@stsci.edu, jrossa@stsci.edu, boeker@stsci.edu

J. CHRISTOPHER MIHOS[3]
Department of Astronomy, Case Western Reserve University, 10900 Euclid Avenue, Cleveland, OH 44106
hos@burro.astr.cwru.edu

JOHN E. HIBBARD
National Radio Astronomy Observatory, 520 Edgemont Road, Charlottesville,VA 22903-2475
jhibbard@nrao.edu

AND

ANN I. ZABLUDOFF
Steward Observatory, University of Arizona, 933 North Cherry Avenue, Tucson, AZ 85721-0065
azabludoff@as.arizona.edu

## ABSTRACT

We report on the properties of nuclear regions in the Toomre Sequence of merging galaxies, based on imaging data gathered with the *Hubble Space Telescope* WFPC2 camera. We have imaged the 11 systems in the proposed evolutionary merger sequence in the F555W and F814W broad-band filters, and in H$\alpha$+[N II] narrow-band filters. The broad-band morphology of the nuclear regions varies from non-nucleated starburst clumps through dust-covered nuclei to a nucleated morphology. There is no unambiguous trend in the morphology with merger stage. The emission-line morphology is extended beyond the nucleus in most cases, but centrally concentrated (within 1 kpc) emission-line gas can be seen in the four latest-stage merger systems. We have quantified the intrinsic luminosity densities and colors within the inner 100 pc and 1 kpc of each identified nucleus. We find little evidence for a clear trend in nuclear properties along the merger sequence, other than a suggestive rise in the nuclear luminosity density in the most evolved members of the sequence. The lack of clear trends in nuclear properties is likely due both to the effects of obscuration and geometry, as well as the physical variety of galaxies included in the Toomre Sequence.

*Subject headings:* galaxies: nuclei — galaxies: interactions — galaxies: evolution — galaxies: spiral — galaxies: formation

## 1. INTRODUCTION

Disk galaxy mergers are believed to be responsible for triggering a variety of global *and* nuclear responses in galaxies. The global effects have been well documented, both with observations, starting with Zwicky's extensive work (1950, 1956, 1964), and with numerical simulations, first convincingly demonstrated by Toomre & Toomre (1972). Work during the last decades strongly suggests that a fraction of elliptical galaxies has formed as a result of disk galaxy merging (see Schweizer 1998, and references therein). The morphology of tidal tails has been used to trace the mass distribution in galactic halos (Dubinski, Mihos, & Hernquist 1996; Mihos, Dubinski, & Hernquist 1998; Springel & White 1999), and the tails themselves are possible birthplaces of some dwarf galaxies (Barnes & Hernquist 1992; Elmegreen et al. 1993; Duc & Brinks 2001). Mergers have also been closely connected to lumi-

nous and ultraluminous infrared galaxies (Lonsdale, Persson, & Matthews 1984; Joseph & Wright 1985; Schweizer 1990; Sanders et al. 1988a; Scoville et al. 2000; Borne et al. 2000).

Perhaps the most dramatic physical process associated with disk galaxy merging is the inflow of gas into the nuclear region and the consequent excitation of nuclear starburst and AGN activity. This process has been reported from simulations (Barnes & Hernquist 1991; Mihos & Hernquist 1994a; Barnes & Hernquist 1996) and from observations (Joseph & Wright 1985; Sanders et al. 1988a; Hutchings & Neff 1992; Bahcall, Kirhakos & Schneider 1995; Surace, Sanders & Evans 2001). Whether the gas "hangs up" and forms stars in the inner kiloparsec, or continues to flow inward towards a putative AGN, has a strong impact on the luminosity and evolution of the merger. The details of the nuclear gasdynamics will depend on

---

the structure of the host galaxies and the dynamical stage of the interaction (Mihos & Hernquist 1996; Barnes & Hernquist 1996). Several scenarios have been suggested in which interactions evolve from starburst-dominated to AGN-dominated regimes as the galaxies merge (Weedman 1983; Sanders et al. 1988a; Veilleux et al. 1995).

Unfortunately, until now, both observations and numerical simulations have lacked the spatial resolution needed to study the evolution of the merging nuclei on scales smaller than a few hundred parsecs. For this reason, our understanding of how mergers fuel nuclear starburst and AGN activity, and drive galaxy evolution from the nucleus out, has remained woefully incomplete. Theoretical arguments suggest that the evolution of the merging nuclei is where the merger hypothesis for the formation of elliptical galaxies through disk galaxy mergers faces its most stringent test.

A wide variety of physical processes may shape the nuclei. Purely stellar dynamical merging alone would tend to produce diffuse nuclei with large cores and a very shallow nuclear surface brightness gradient (Hernquist 1992) unless the progenitor nuclei were dense (Barnes 1988). In the case of gas-rich disk galaxies, the dissipative flow of gas into the nuclei and accompanying star formation would tend to result in a steep luminosity profile (Mihos & Hernquist 1994b) and a large central density, as seen in several young merger remnants (R. P. van der Marel et al., in preparation; see also figure 2 in van der Marel & Zurek 2000). The presence of a central supermassive black hole would also induce a strong nuclear power-law cusp (Young 1980; Quinlan, Hernquist, & Sigurdsson 1995). Yet if both galaxies contain supermassive central black holes which merge, the resulting black hole binary would act as a dynamical slingshot and eject stars from the center, thus lowering the stellar density there (Quinlan & Hernquist 1997; Milosavljević & Merritt 2001).

For these reasons we are undertaking a high resolution *Hubble Space Telescope (HST)* survey of the nuclear regions in a sequence of merging galaxies. The questions we want to answer include the following: 1. What is the morphology of the ionized gas distribution around the nucleus? Is it clumpy, diffuse and extended, ring-like, or compact and disk-like? Does this morphology depend on the interaction stage? 2. How is the current star formation, as revealed by the Hα line emission, distributed with respect to the young stellar populations as revealed by their blue color (and, eventually, spectra)? 3. How do the nuclear starbursts affect the radial color gradients of the merger remnants? The spatial resolution of the *HST* (10–50 pc in nearby systems) is required to investigate these questions, which are the focus of the current paper. In future papers, we will study the stellar populations, kinematics, and evolution of the merger-induced starbursts of the Toomre Sequence nuclei, using *HST* STIS spectra and NICMOS imaging.

## 2. GALAXY SAMPLE AND OBSERVATIONS

### 2.1. *Sample*

The Toomre Sequence (Toomre 1977) is a sample of 11 relatively nearby (within ∼120 Mpc) interacting and merging disk galaxies, which have been arranged into a sequence according to the *putative* time before or since merging. These systems were chosen because they exhibit conspicuous tidal tails and "main bodies that are nearly in contact or perhaps not even separable" (Toomre 1977). They span a range of dynamical phases, from galaxies early in the merging process (e.g., NGC 4038/39 and NGC 4676) to late-stage merger remnants (e.g., NGC 3921 and NGC 7252; see Figure 1 and Table 1). We want to emphasize the word "putative", since the placing of a system in this sequence was based on the apparent degree of coalescence of the progenitor main bodies in low-resolution optical photographical plates, assuming that the progenitors resembled normal disk galaxies in the pre-encounter stage.

Because of the requirement of well-developed tidal tails, these systems have suffered, or are suffering, encounters that are most likely of prograde sense (with the disks rotating in the same sense as they orbit each other). In such a scenario, the orbits of interacting galaxies decay as the galaxies lose orbital energy and angular momentum via dynamical friction with their dark halos. Ultimately, the galaxies coalesce and form a single merger remnant. On these grounds we can call the Toomre Sequence an evolutionary sequence. Because it is an *optically* selected sample of merging galaxies, it suffers less from dust obscuration than infrared-luminous samples, allowing the nuclei to be studied at optical wavelengths. The Toomre Sequence has been widely investigated by ground-based observations (Joseph & Wright 1985; Stanford & Bushouse 1991; Hibbard & van Gorkom 1996; Schweizer 1998; Yun & Hibbard 2001; Georgakakis et al. 2000), space-based observations (Fabbiano et al. 1997; Read & Ponman 1998; Awaki et al. 2002; Zezas et al. 2002a,b), and numerical studies (Toomre & Toomre 1972; Barnes 1988; Stanford & Balcells 1991; Mihos et al. 1993; Hibbard & Mihos 1995; Barnes 1998).

### 2.2. *Observations and Data Reduction*

All images were taken with the WFPC2 camera onboard the *HST*. We used the F555W and F814W filters, which mimic the better-known *V*- and *I*-bands, with integration times of 320 seconds in each band, split into two exposures of 160 seconds to allow for cosmic ray rejection (see Table 2 for more information on the exposure times). Images in these bands for NGC 4038/39 (Whitmore et al. 1999), NGC 3921 (Schweizer et al. 1996), and NGC 7252 (Miller et al. 1997) already existed in the *HST* archive. We used those images in our current study. Narrow-band images covering the Hα+[N II] lines were taken with the F673N narrow-band filter in cases where the line emission from the target fell within the wavelength range covered by this filter (NGC 3509; NGC 7592), or otherwise with the Linear Ramp Filter (LRF). The LRFs have a bandwidth of about 1.3% of the central wavelength. The position of the galaxy on the CCD chip depends on the central wavelength and limits the field of view to about $10'' \times 10''$ for the LRF. The list of the adopted filters, central wavelengths, and FWHM values of the filters together with integration times are given in Table 2. The Antennae, NGC 4038/39, was imaged earlier in the *HST* F658N Hα filter by Whitmore et al. (1999), and we used these data in our work.

We employed the STSDAS task WFIXUP to interpolate (in the x-direction) over bad pixels as identified in the data
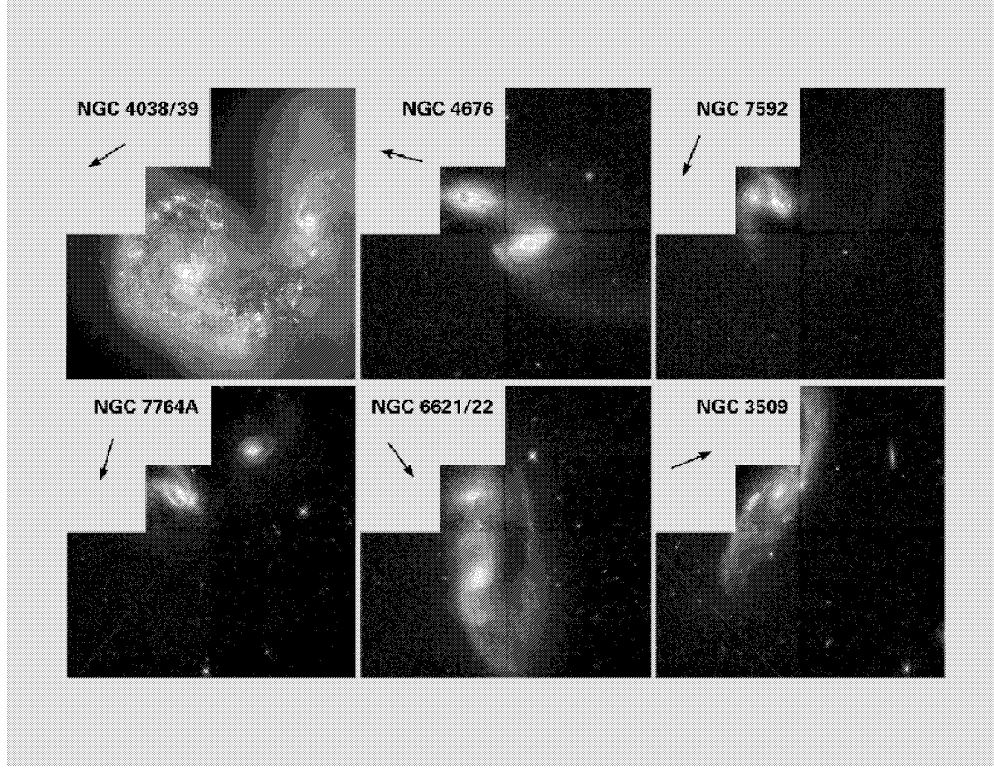
FIG. 1.— Color composite, mosaiced F555W- and F814W-band images of the Toomre Sequence of merging galaxies, ordered from top left to bottom right in the original order of Toomre (1977). The arrow in each sub-panel indicates the North direction. The visible trails in the NGC 7764A and NGC 3509 images are most probably satellite tracks.

TABLE 1

THE TOOMRE SEQUENCE.

| Sequence Number | Galaxy | R.A. (J2000.0)[a] (hh mm ss.ss) | Dec. (J2000.0)[a] (dd°mm′ss″s) | $cz$[b] (km s$^{-1}$) | Dist.[c] (Mpc) | $\theta_{nuc}$[d] (″) | 0″1[e] (pc) | Dynamical Model[f] |
|---|---|---|---|---|---|---|---|---|
| 1. | NGC 4038 | 12 01 53.06 | −18 52 01.3 | 1616 | 21.6 | 61.4 | 10 | Y[g] |
| 1. | NGC 4039 | 12 01 53.54 | −18 53 09.3 | 1624 | 21.6 | 61.4 | 10 | Y[g] |
| 2. | NGC 4676 NUC1 | 12 46 10.06 | +30 43 55.5 | 6613 | 88.2 | 37.1 | 43 | Y[h] |
| 2. | NGC 4676 NUC2 | 12 46 11.17 | +30 43 21.2 | 6613 | 88.2 | 37.1 | 43 | Y[h] |
| 3. | NGC 7592 NUC1 | 23 18 21.73 | −04 24 56.7 | 7280 | 97.1 | 13.0 | 47 | N |
| 3. | NGC 7592 NUC2 | 23 18 22.60 | −04 24 57.3[i] | 7280 | 97.1 | 13.0 | 47 | N |
| 4. | NGC 7764A | 23 53 23.74 | −40 48 26.3 | 9162 | 122.2 | 0 | 59 | N |
| 5. | NGC 6621 | 18 12 55.25 | +68 21 48.5 | 6191 | 84.4 | 41.7 | 41 | N |
| 5. | NGC 6622 | 18 12 59.74 | +68 21 15.1 | 6466 | 84.4 | 41.7 | 41 | N |
| 6. | NGC 3509 | 11 04 23.59 | +04 49 42.4 | 7704 | 102.7 | 0 | 50 | N |
| 7. | NGC 520 NUC1 | 01 24 34.89 | +03 47 29.9 | 2281 | 30.4 | 40.3 | 15 | Y[j] |
| 7. | NGC 520 NUC2 | 01 24 33.30 | +03 48 02.4 | 2281 | 30.4 | 40.3 | 15 | Y[j] |
| 8. | NGC 2623 | 08 38 24.11 | +25 45 16.6 | 5535 | 73.8 | 0 | 36 | N |
| 9. | NGC 3256 | 10 27 51.17 | −43 54 16.1 | 2738 | 36.5 | 0 | 18 | N |
| 10. | NGC 3921 | 11 51 06.96 | +55 04 43.1 | 5838 | 77.8 | 0 | 38 | N |
| 11. | NGC 7252 | 22 20 44.78 | −24 40 41.8 | 4688 | 62.5 | 0 | 30 | Y[k] |

[a]Coordinates refer to the measured positions of the nuclei in our WFPC 2 images, except for Nuc 1 in NGC 520 where it was measured from a ground-based $K$-band image (no clear nuclear position could be determined in our *HST* images).

[b]Heliocentric velocity, data taken from the NASA Extragalactic Database (NED), except for NGC 4676, for which the value was taken from the Lyon Extragalactic Database (LEDA).

[c]Distance for H$_0$ = 75 km s$^{-1}$ Mpc$^{-1}$. In cases where the two components have different systemic velocities, the distance to both is the average of the two Hubble law distances.

[d]Nuclear separation in arcseconds, calculated from the listed positions.

[e]Spatial scale in pc corresponding to 0″1.

[f]Dynamical model means that an N-body simulation that tries to reproduce the observed structure and kinematics of the merger exists.

[g]Barnes 1988.

[h]Barnes 1998.

[i]The position of Nuc 2 in NGC 7592 is highly uncertain, as it is very difficult to determine the location of the nucleus in the optical images.

[j]Stanford & Balcells 1991.
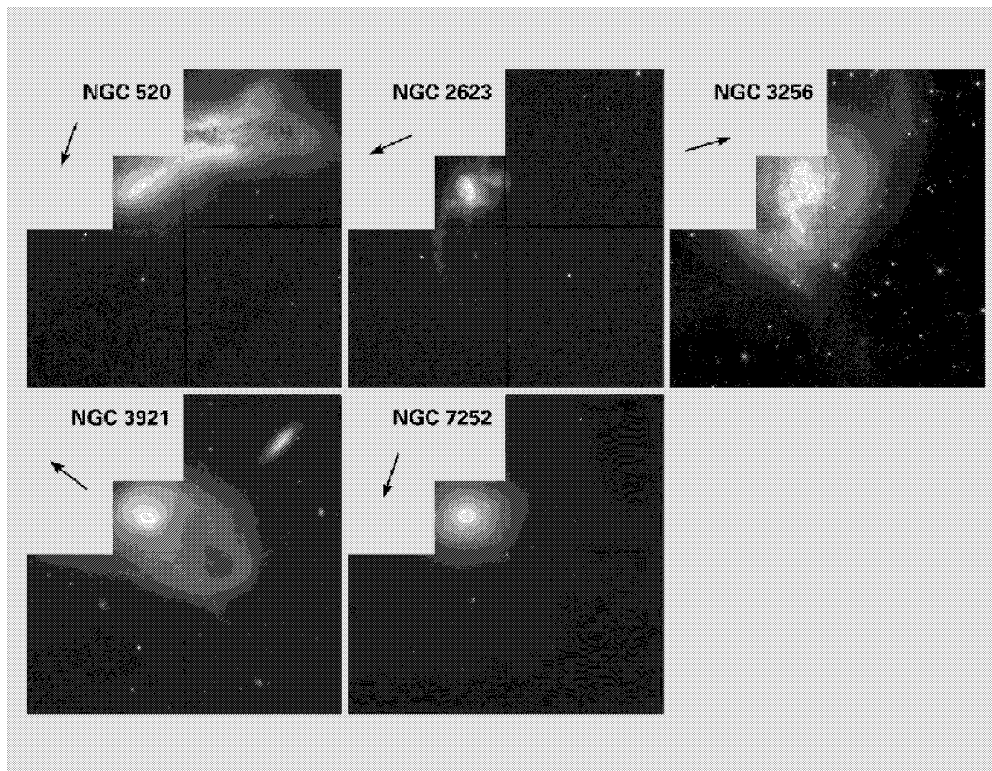
[k]Hibbard & Mihos 1995.

Fig. 1.— Continued.

quality files. We also used the STSDAS task WARMPIX to correct consistently warm pixels in the data, using the most recent warm pixel tables. The STSDAS task CR-REJ was used to combine the two 160 second exposures. This step corrects most of the pixels affected by cosmic rays in the combined image. In general, a few cosmic rays remain uncorrected, mostly when the same pixel was hit in both exposures. Also, a small number of hot pixels remain uncorrected because they are not listed even in the most recent warm pixel tables. We corrected these with the IRAF task COSMICRAYS, setting the "threshold" and "fluxratio" parameters to values selected by a careful comparison of the images before and after correction, to ensure that only questionable pixels were replaced. The rest of the reduction was done with the standard WFPC2 pipeline tasks using the best reference files available. The LRF exposures were flat-fielded using the narrow-band F656N and F673N (whichever was closer in wavelength) flat fields. We also created mosaiced F555W and F814W images with the IRAF/STSDAS task WMOSAIC. Color composite mosaics of these images, which show the environment around the nuclei, and tidal tails in some systems, are displayed in Figure 1.

The photometric calibration, and conversion to Johnson $V$- and $I$-bands was performed according to guidelines in Holtzman et al. (1995). A $K$-correction has not been applied to any of our measurements. Since the throughput of the narrow-band filters does not vary much at the wavelengths of the lines, it was possible to calibrate the line fluxes by assuming zero width for the lines (monochromatic). We used the IRAF/STSDAS SYNPHOT task BANDPAR to compute the conversion from counts sec$^{-1}$ to ergs sec$^{-1}$ cm$^{-2}$. The results were the same within er-

rors to those produced by the SYNPHOT task CALCPAR.

Using the known relative orientation of the various chips on WFPC2, we rotated the chips which contained the line emission and the PC-chip $V$ and $I$ images to the same orientation. We used stars in the images to register the frames. The final emission-line images were constructed by accounting for the different scales of images on various chips (usually the PC chip and WF2 chip), and scaling down the $V$- and $I$-band images to the expected count levels corresponding to the wavelength and band of the line image, with the help of the WFPC2 exposure time calculator. We then combined the broad-band images by taking their geometric mean and performed a final adjustment to this combined continuum image by selecting areas well outside emission-line regions (with pure stellar emission) and comparing fluxes in corresponding areas in the continuum and line images. Finally, we subtracted the scaled continuum image from the line image. Using the combination of $V$ and $I$ images eliminates the extinction terms in the case of foreground extinction, as explained in detail by Verdoes Kleijn et al. (1999). In some cases, the residual image shows negative pixels, which are most likely due to strong color gradients near the nuclei. We estimate that the final uncertainty in the line fluxes is no better than 50%, based on varying the scaling of the continuum image within acceptable limits and comparing the derived total line fluxes.

Color index images were created by dividing the F555W image by the F814W image, taking the logarithm of the result, and correcting for differences in the color terms, using the synthetic calibration from Holtzman et al. (1995). For our new imagery (i.e., all systems except NGC 4038/39, NGC 3921, and NGC 7252), many regions in the raw

Table 2

WFPC2 EXPOSURES WITH THE CORRESPONDING CHIP ON WHICH THE NUCLEI ARE CENTERED, AND INTEGRATION TIMES.

| Object | Chip | Filter | $\lambda_0$[a] | $\Delta\lambda$[b] | $t$(sec)[c] |
|---|---|---|---|---|---|
| NGC 4038/39[d] | WF2/WF4 | F555W | 5407 | 1223 | 4 × 1100 |
| NGC 4038/39[d] | WF2/WF4 | F814W | 5407 | 1223 | 4 × 500 |
| NGC 4038/39[d] | WF2/WF4 | F658N | 6591 | 28.5 | 3800 |
| NGC 4676 Nuc 1 | PC1 | F555W | 5407 | 1223 | 2 × 160 |
| NGC 4676 Nuc 1 | PC1 | F814W | 7940 | 1758 | 2 × 160 |
| NGC 4676 Nuc 1 | WF2 | LRF | 6715.3 | 80.1 | 2 × 600 |
| NGC 4676 Nuc 2 | PC1 | F555W | 5407 | 1223 | 2 × 160 |
| NGC 4676 Nuc 2 | PC1 | F814W | 7940 | 1758 | 2 × 160 |
| NGC 4676 Nuc 2 | WF2 | LRF | 6714.4 | 79.9 | 2 × 600 |
| NGC 7592 | PC1 | F555W | 5407 | 1223 | 2 × 160 |
| NGC 7592 | PC1 | F814W | 7940 | 1758 | 2 × 160 |
| NGC 7592 | WF2 | F673N | 6732 | 47.2 | 2 × 600 |
| NGC 7764A | PC1 | F555W | 5407 | 1223 | 2 × 160 |
| NGC 7764A | PC1 | F814W | 7940 | 1758 | 2 × 160 |
| NGC 7764A | WF2 | LRF | 6770.8 | 84.2 | 2 × 600 |
| NGC 6621 | PC1 | F555W | 5407 | 1223 | 2 × 160 |
| NGC 6621 | PC1 | F814W | 7940 | 1758 | 2 × 160 |
| NGC 6621 | WF2 | LRF | 6706.2 | 79.3 | 2 × 700 |
| NGC 6622 | PC1 | F555W | 5407 | 1223 | 2 × 160 |
| NGC 6622 | PC1 | F814W | 7940 | 1758 | 2 × 160 |
| NGC 6622 | WF2 | LRF | 6711.5 | 79.9 | 2 × 700 |
| NGC 3509 | PC1 | F555W | 5407 | 1223 | 2 × 160 |
| NGC 3509 | PC1 | F814W | 7940 | 1758 | 2 × 160 |
| NGC 3509 | PC1 | F673N | 6732 | 47.2 | 2 × 600 |
| NGC 520 Nuc 1 | PC1 | F555W | 5407 | 1223 | 2 × 160 |
| NGC 520 Nuc 1 | PC1 | F814W | 7940 | 1758 | 2 × 160 |
| NGC 520 Nuc 1 | PC1 | LRF | 6619.2 | 75.5 | 2 × 600 |
| NGC 520 Nuc 2 | PC1 | F555W | 5407 | 1223 | 2 × 160 |
| NGC 520 Nuc 2 | PC1 | F814W | 7940 | 1758 | 2 × 160 |
| NGC 520 Nuc 2 | PC1 | LRF | 6617.1 | 75.8 | 2 × 600 |
| NGC 2623 | PC1 | F555W | 5407 | 1223 | 2 × 160 |
| NGC 2623 | PC1 | F814W | 7940 | 1758 | 2 × 160 |
| NGC 2623 | WF2 | LRF | 6691.4 | 78.6 | 2 × 600 |
| NGC 3256 Nuc 1 | PC1 | F555W | 5407 | 1223 | 2 × 160 |
| NGC 3256 Nuc 1 | PC1 | F814W | 7940 | 1758 | 2 × 160 |
| NGC 3256 Nuc 1 | WF2 | LRF | 6631.4 | 75.9 | 2 × 600 |
| NGC 3256 Nuc 2 | PC1 | F555W | 5407 | 1223 | 2 × 160 |
| NGC 3256 Nuc 2 | PC1 | F814W | 7940 | 1758 | 2 × 160 |
| NGC 3256 Nuc 2 | WF2 | LRF | 6631.4 | 75.9 | 2 × 600 |
| NGC 3921[e] | PC1 | F555W | 5407 | 1223 | 2 × 1200 |
| NGC 3921[e] | PC1 | F814W | 7940 | 1758 | 2 × 900 |
| NGC 3921 | WF2 | LRF | 6698.9 | 79.0 | 2 × 700 + 800 |
| NGC 7252[f] | PC1 | F555W | 5407 | 1223 | 3600 |
| NGC 7252[f] | PC1 | F814W | 7940 | 1758 | 2400 |
| NGC 7252 | WF2 | LRF | 6673.9 | 77.9 | 2 × 700 + 600 |

[a]Central wavelength in Å [from the WFPC2 Handbook, Table 3.1 Biretta et al. (2000), for the standard filters; as specified in the observations for the LRF filters].

[b]Filter width in Å [from the WFPC2 Handbook, Table 3.1 Biretta et al. (2000), for the standard filters; equivalent Gaussian FWHM from the IRAF CALCPHOT task for the LRF filters].

[c]Integration time.

[d]Data from Whitmore et al. 1999.

[e]Data from Schweizer et al. 1996.

[f]Data from Miller et al. 1997.

color index images are of low signal-to-noise. We therefore constructed smoothed color index maps using an adaptive filtering procedure, as described by Scoville et al. (2000), where areas with lower signal-to-noise ratios were smoothed by a larger boxcar. These images were then masked so as to only show areas with adequate signal-to-noise (signal-to-noise greater than two in both $V$- and $I$-images after being smoothed with an $11\times11$ pixel boxcar median filter). The resulting smoothed color index images, together with the unsmoothed broad-band images and H$\alpha$+[N II] images, are shown in Figures 2–16.

### 3. GALAXY MORPHOLOGY

In the following we give a brief description of each system, based on Figures 2–16, together with a few references to earlier work. We use a Hubble constant of $H_0 = 75 \, \mathrm{km \, s^{-1} \, Mpc^{-1}}$ throughout this paper.

#### 3.1. *NGC 4038 and NGC 4039 (The Antennae)*

Perhaps the best-known system in the sequence is the Antennae. We use the spectacular $HST$ $V, I$, and H$\alpha$ images of this system from Whitmore et al. (1999; see also Whitmore & Schweizer 1995 and Figure 1). These images show the chaotic dust lanes and prevalent star formation in the interface between the two galaxies. They also reveal the redder color of the underlying population in the bulge component of each galaxy. The focus of the Whitmore et al. papers was on the abundant young star clusters which have apparently formed as the result of the interaction of the two galaxies. The properties and evolution of such clusters in a merger event have been discussed extensively in a series of papers by Whitmore and his collaborators (e.g., Whitmore & Schweizer 1995; Schweizer et al. 1996; Miller et al. 1997; Whitmore et al. 1997, 1999; Zhang, Fall, & Whitmore 2001). The nuclear regions of merging galaxies are potential formation sites of new super star clusters (Bekki & Couch 2001). We instead investigate the morphology and star formation activity in the central few hundred parsecs.

The nuclear region of the northern component of the Antennae, NGC 4038, is bracketed by star clusters in the $V$ and $I$ images. The position of the nucleus is most likely near the knot "J" in the classification scheme of Whitmore & Schweizer (1995), and close to the nuclear position identified in the radio continuum by Zhang et al. (2001; using the radio continuum data of Neff & Ulvestad 2000) and in the near-infrared by Mengel et al. (2001). In our I-band image, this is located near the center of the frame displayed in Fig. 2. There we see an elongated ring-like structure, with an axis ratio of about 0.3 and a diameter of about 2.5 (260 pc), pointing north-northeast. The coordinates of the optical knot that we identified as the nucleus of NGC 4038 in the WFPC2 images are given in Table 1. They agree with the radio continuum position to within one arcsecond and they are within about 3 arcseconds of the estimated near-infrared position of the nucleus. The absolute accuracy of the coordinates reported in this paper is $\sim 1''$. This is the intrinsic accuracy of the $HST$ guide star coordinate system. The H$\alpha$ image (see Fig. 2) also shows the elongated ring structure with a peak in the north-northeastern corner at the position of the star clusters seen in the $V$- and $I$-band images. The $V - I$

colors of the clusters in the ring-like structure vary from 0.4 to 1.0, while a typical color outside and inside the ring is 1.5, reaching up to 1.9 in the dust lanes. Most of the dust is concentrated on the southeastern side of the elongated ring-like structure. Near-infrared high resolution $HST$ NICMOS observations of the nucleus will be reported in a future paper. They promise to shed more light on the issue of the true location of the nucleus in NGC 4038. Previous ground-based near-infrared imaging (Bushouse & Werner 1990; Hibbard et al. 2001; Mengel et al. 2001) does not have high enough spatial resolution to indicate the exact location of the nucleus.

The nucleus of NGC 4039, the southern component of the Antennae, is much easier to recognize in the $V$ and $I$ images (see Fig. 3). Our identified nuclear position (the position of the optical peak) in Table 1 agrees to within about two arcseconds of the estimated nuclear positions from the radio continuum data (Zhang et al. 2001) and near-infrared data (Mengel et al. 2001). The nucleus is surrounded by dust patches and dust lanes. There is also a minor peak of H$\alpha$ emission at the location of the nucleus, which could be due to continuum subtraction uncertainties. Much more intense H$\alpha$ emission is seen in the arm connecting to the nucleus. The $V - I$ color of the nucleus of NGC 4039 is about 1.0, and the surrounding area has a color around 1.3, with values of 1.7 in a dusty region close to the nucleus.

Neither NGC 4038 nor NGC 4039 is classified as a Seyfert or LINER nucleus. These nuclei are instead hosts of mild starbursts (e.g., Dahari 1985; Véron–Cetty & Véron 1986). Further evidence for the starburst nature of these nuclei comes from X-ray observations with the ROSAT High-Resolution Imager (Fabbiano et al. 1997) and with Chandra (Zezas et al. 2002a,b). The northern X-ray nucleus (NGC 4038) has a soft spectrum, which hints at thermal emission and is probably related to a hot wind, whereas the thermal + power-law spectrum of the southern X-ray nucleus (NGC 4039) indicates a hot ISM and a contribution from X-ray binaries.

#### 3.2. *NGC 4676 (The Mice)*

The Mice is a pair of spiral galaxies with only moderately active nuclei (classified as LINER-type by Keel et al. 1985). The nucleus of NGC 4676A or Nuc 1 (the northern component of the pair) is covered by dust in our optical $V$ and $I$ images (Fig. 4). This dust is likely associated with the dense edge-on molecular disk imaged in CO(1-0) by Yun & Hibbard (2001). Adopting standard conversion factors, the observed peak CO flux density suggests that the nucleus of NGC 4676A is hidden beneath $A_V \sim 60$ magnitudes of extinction.

Just south of the area of heavy dust obscuration near the base of the northern tail is a V-shaped structure (with the V being sideways and opening to the east, and the tip of the V at R.A. $12^\mathrm{h}46^\mathrm{m}10\overset{s}{.}1$ and Dec. $30°43'55\overset{''}{.}0$) of brighter emission from young stellar clusters near the center of the main body. About $7''$ (3 kpc) to the south one can see a triangle-shaped structure of young clusters. The tip of the central V-shaped cluster lies near the peak emission in a ground-based K' image (J. Hibbard, unpublished; see also Bushouse & Stanford 1992), so we assume that the nucleus lies near this position. The H$\alpha$ emission
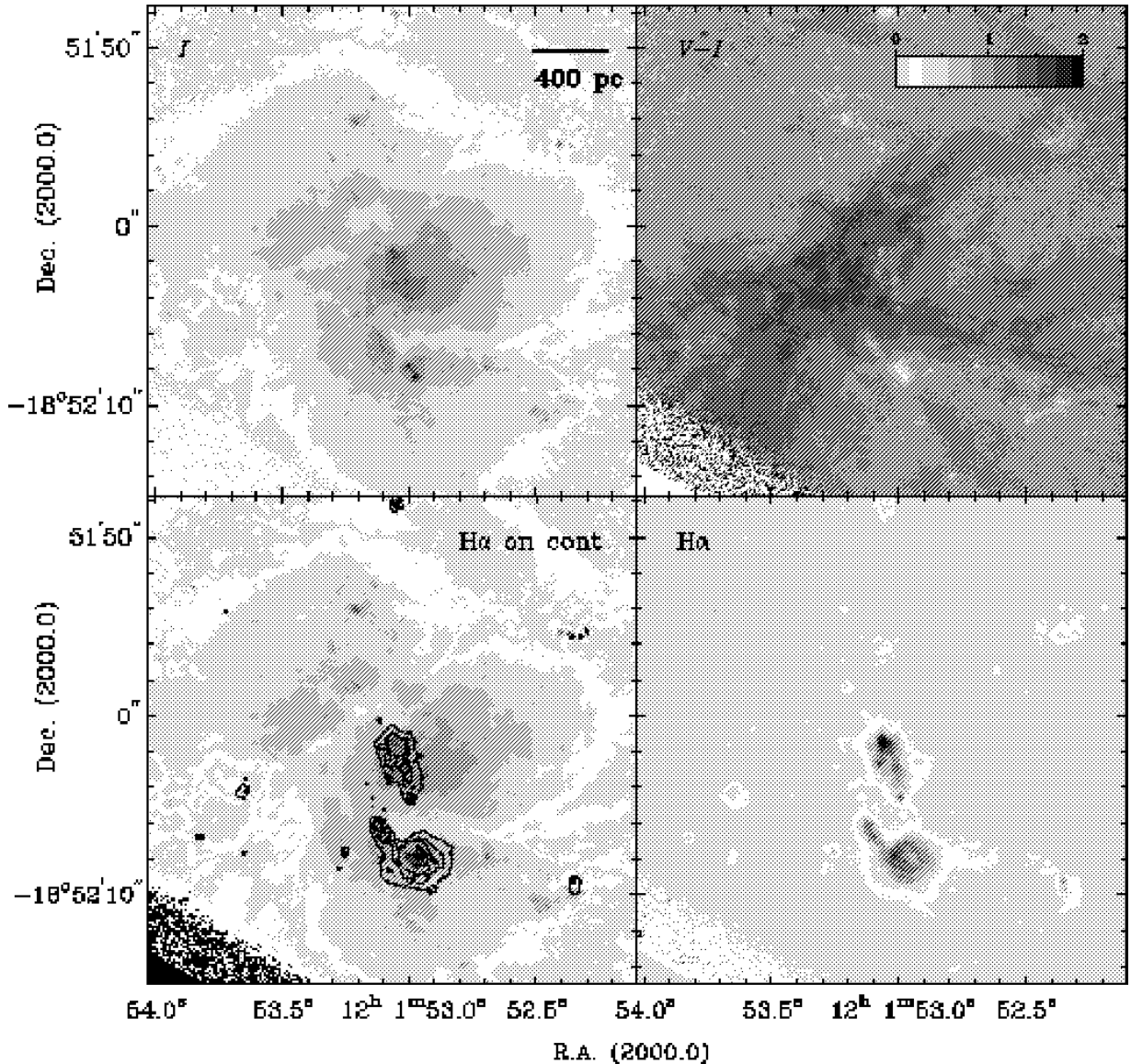
FIG. 2.— NGC 4038. Upper left: $I$ image. Upper right: $V - I$ color index image. Lower left: continuum (gray-scale) and H$\alpha$ + [N II] (contours) image. Lower right: H$\alpha$ gray-scale image. The gray-scale levels are arbitrary and were adjusted to show details in the nuclear region. The H$\alpha$ contour levels in the lower left image are at (10%, 30%, 50%) of $7.2 \times 10^{-17}$ ergs s$^{-1}$ cm$^{-2}$ per pixel. North is up and east is to the left in this and in the subsequent galaxy images.

from NGC 4676A is weak. In general, the emission is elongated in the north–south direction of the main body. The V-shaped structure has very red $V - I$ colors above 2.2. Perhaps even more surprisingly, the color of the heavily extinguished dust patch near the base of the tail is actually *bluer* than its surroundings, having an average $V - I$ value less than 1. We interpret this region as scattered light from young stars which are mostly hidden by the dust. A hint of this young star population is seen in the $V$ image (not shown here). Such a young star forming region can be seen even more clearly in the new, deeper ACS images of the Mice (Ford et al. 2002). In contrast to the V-shaped structure, the triangle-shaped structure of clusters near the southern end of the main body has bluer colors than its surroundings, with $V - I$ values around 1 or slightly below it.

The nucleus is easily identified in NGC 4676B or Nuc 2. It is surrounded by a rather amorphous disk, and a dust

lane that seems to wrap around the whole disk, ending near the location of the nucleus (Fig. 5). There is a peak of H$\alpha$ emission offset by about 0.''2 from the nucleus of NGC 4676B, but in general the H$\alpha$ emission is weak and patchy. The nucleus has $V - I$ colors close to 1.3. A dust patch near the nucleus has a $V - I$ color as red as 1.7. The majority of the disk outside the dust lanes and dust patches has a $V - I$ color of 1.2–1.3. The overall appearance of NGC 4676B, particularly the well-defined bulge/nucleus, is consistent with it being of an earlier Hubble-type than its interacting partner, NGC 4676A (Yun & Hibbard 2001).

### 3.3. *NGC 7592*

This is the third most distant system in the Toomre Sequence, and the main bodies of both galaxies fit within the PC chip of the WFPC2. NGC 7592A or Nuc 1, further to the west, has an active Seyfert 2 nucleus, whereas
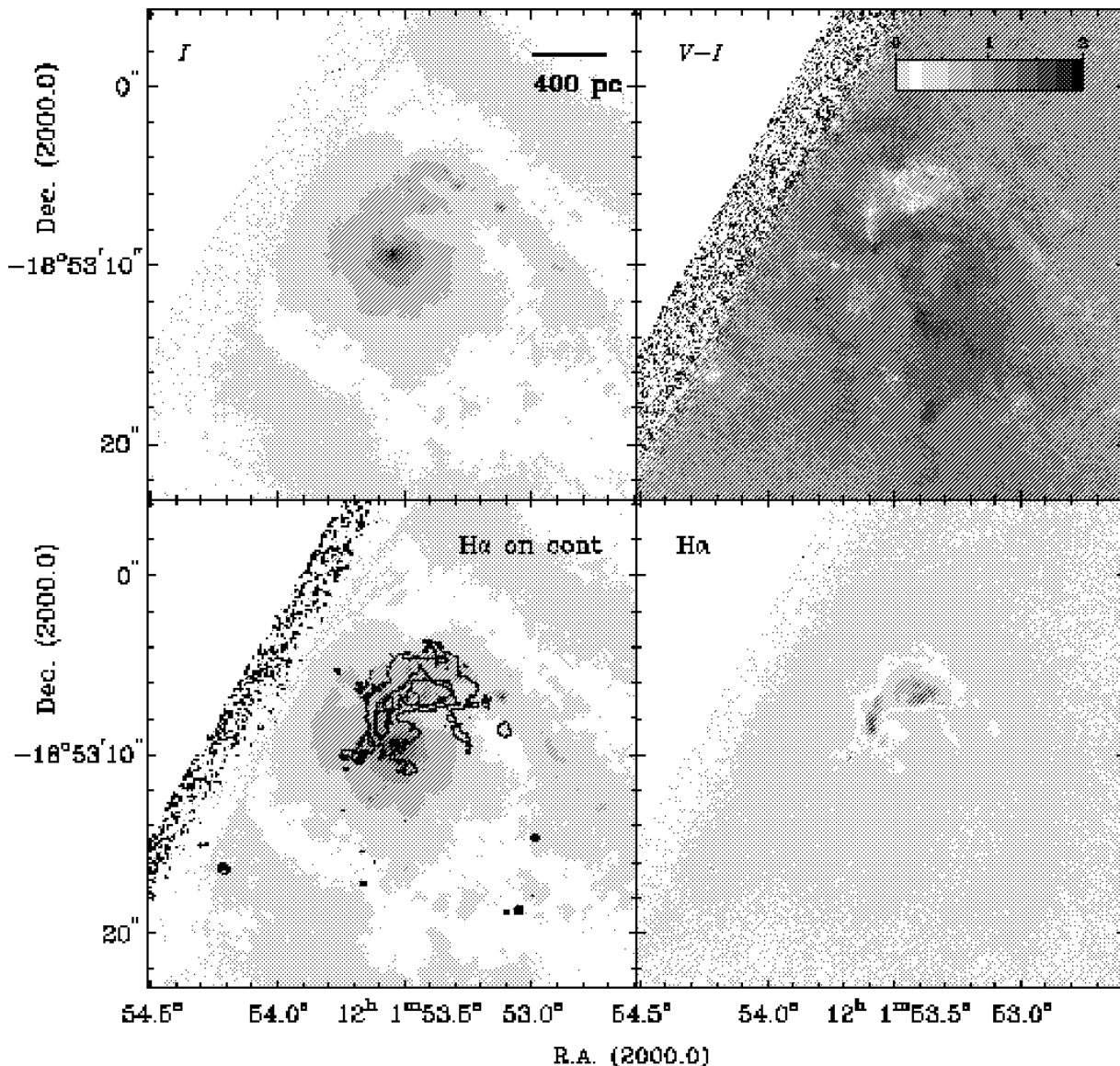
FIG. 3.— NGC 4039, as in Figure 2. The H$\alpha$ contour levels in the lower left image are at (10%, 30%, 50%) of $7.5\times10^{-17}$ ergs s$^{-1}$ cm$^{-2}$ per pixel.

NGC 7592B or Nuc 2 is classified as a starbursting system (Dahari 1985; Rafanelli & Marziani 1992; Kewley et al. 2001; Hattori et al. 2002). NGC 7592A has a much better defined nucleus or bulge than NGC 7592B, consistent with the suggestion of Hattori et al. (2002), who argue that NGC 7592A is of an earlier Hubble-type than NGC 7592B. Bushouse & Werner (1990) claim that NGC 7592A is seen almost face-on, because of its roundish appearance in ground-based optical and $K$-band images. If so, this galaxy appears to possess a bar-like structure in the bulge, although the bar classification is uncertain due to patchy emission and one-sided dust. Similarly, Bushouse & Werner (1990) argued that NGC 7592B is more highly inclined to the line-of-sight. This, together with its later Hubble-type, explains why no clear nucleus is seen in this system. A comparison to the ground-based $K$-band image of Bushouse & Werner (1990) suggests that the nucleus of NGC 7592B lies near the center of the ring-like structure of bright clumps seen in Figure 6. We are not able to identify any specific clump with the nucleus.

The H$\alpha$ image shows abundant emission around the nucleus and the "bar" of NGC 7592A, and emission from the clumps in the ring of NGC 7592B, with a strong central depression in emission. The nucleus of NGC 7592A has blue colors with $V - I$ around 0.8, contrasting to a dust lane lying on one side of the bar with a $V - I$ color close to 2.0. The southern side of the ring structure in NGC 7592B has very blue colors down to $V - I$ of 0.3, but there is a region of red colors of $V - I$ up to 1.9 in the northern part of the ring. Although there is dust visible at that location as well, the red color may suggest that the underlying red nucleus lies at this location.

### 3.4. NGC 7764A

This is the most distant system in our sample at $D = 122$ Mpc. The location of NGC 7764A in the Toomre Sequence, among galaxies with clearly separate nuclei (Fig. 1) suggests that Toomre thought the nuclei of the two systems
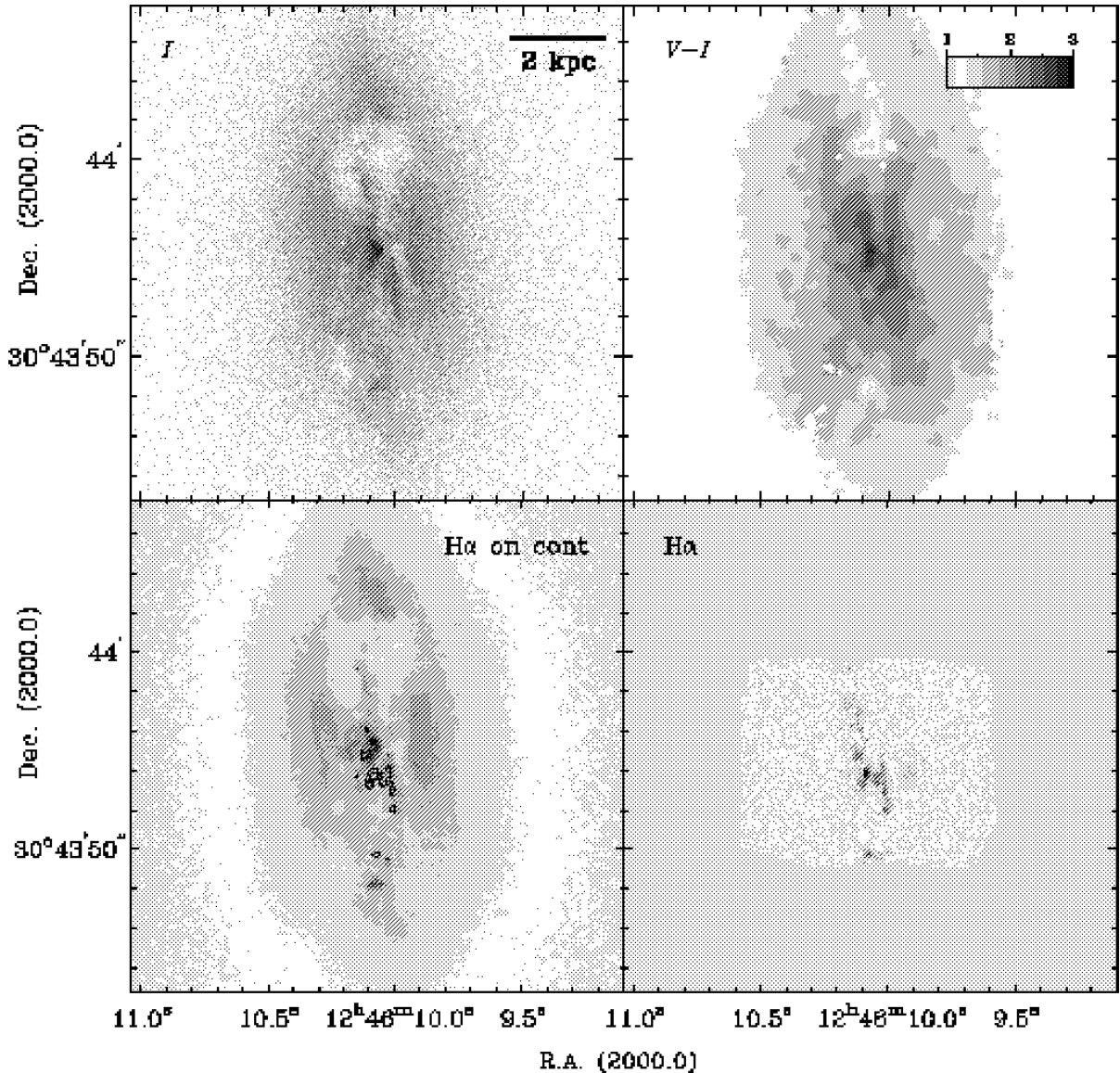
Fig. 4.— NGC 4676A or Nuc 1, as in Figure 2. This color index image and many of the subsequent color index images only show areas where the signal-to-noise ratio was sufficiently high to reveal a meaningful, smooth color. The Hα contour levels in the lower left image are at (20%, 90%) of $1.2\times10^{-16}$ ergs s$^{-1}$ cm$^{-2}$ per pixel.

were still distinct. However, our *HST* images (Figure 7) do not obviously support the presence of two distinct nuclei. Future NICMOS near-infrared data will be critical in identifying the likely remains of the interacting galaxies. For now we only identify one main component from which both the tails are emanating. There is also a barred spiral galaxy, presumably at a similar redshift, displaced about $40''$ (23.7 kpc in projected distance) to the southeast of the main system (imaged on one of our WF chips, see Fig. 1), and a third system with apparent tidal streamers displaced about $40''$ to the northwest, just outside our PC image.

Our PC image reveals a shred or linear feature about $7''$ (4.1 kpc) to the northwest of the main body of NGC 7764A. About a dozen bright, blue ($V - I \sim 0.6$–$0.8$) star clusters lie within this filament. Between this filament and the center of Fig. 7 is a very bright, very blue ($V - I \sim 0.22$) cluster. This cluster has associated Hα emission with a "head-tail" morphology, with the clus-

ter at the "head", and the "tail" pointing to the north-northeast. Following the "head" towards the center of the image in Fig. 7, there is a string of H II regions, crossed by dust lanes. The centralmost H II region is weaker than the regions to its northwest and southeast, and is associated with two adjacent bright optical clusters. These two clusters lie near the region of very red colors in the $V - I$ map, with the reddest region ($V - I \sim 2.4$) associated with the eastern cluster. This strong dust concentration may indicate that this is the location of one of the nuclei. The western clump of the double cluster is bluer ($V - I \sim 1.5$) and brighter.

There are more bright HII regions about $3''$ (1.8 kpc) to the northeast of the double cluster, associated with another bright star cluster embedded in dust. Further to the east of this is an amorphous luminous region with rather blue colors ($V - I \sim 0.6$–$0.8$).
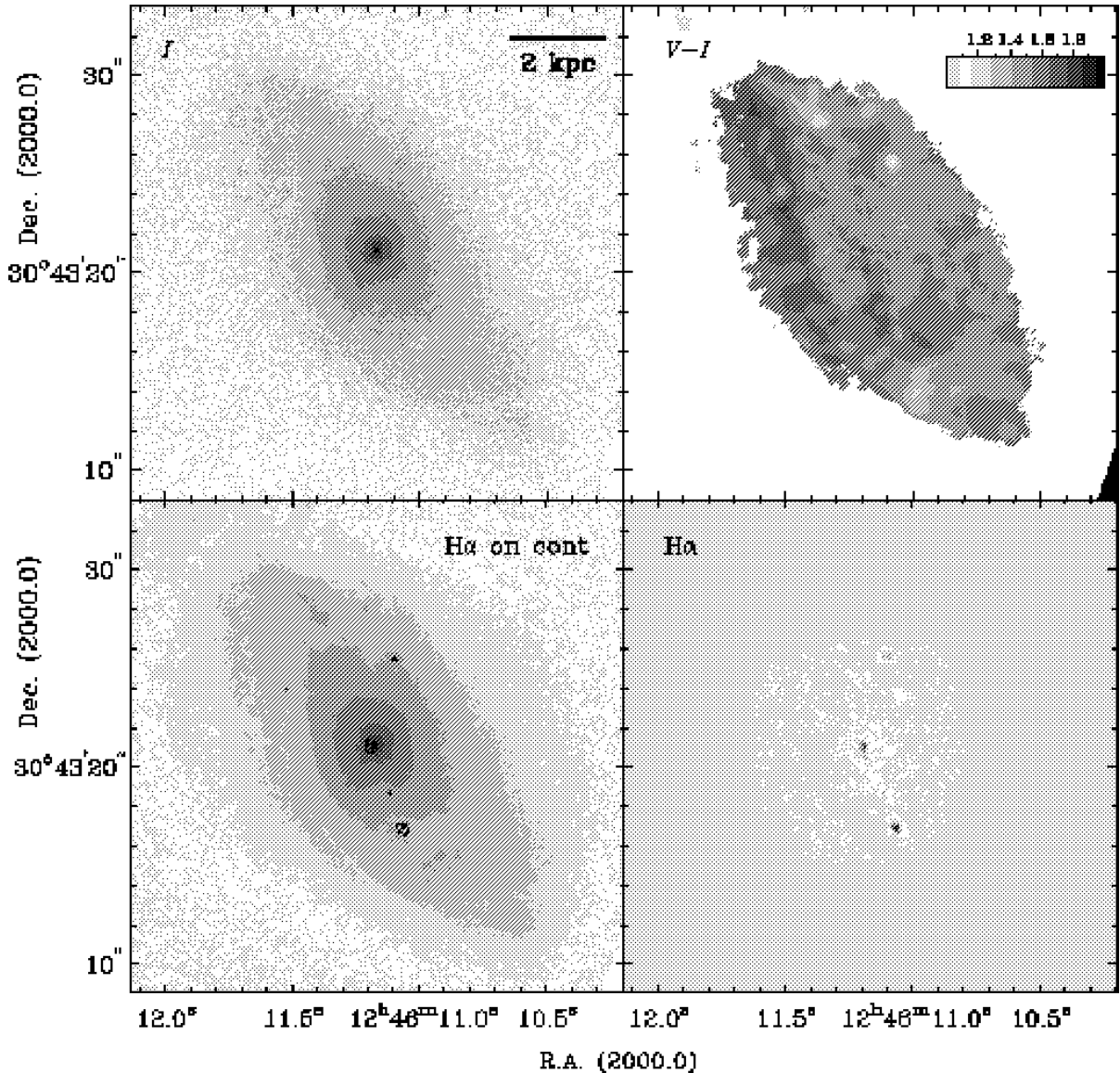
FIG. 5.— NGC 4676B or Nuc 2, as in Figure 2. The Hα contour levels in the lower left image are at (20%, 50%) of $3.8\times10^{-17}$ ergs s$^{-1}$ cm$^{-2}$ per pixel.

### 3.5. NGC 6621 and NGC 6622

The northern component of this interacting galaxy pair, NGC 6621, has a dusty central region punctuated by patchy star clusters and ionized gas emission (Fig. 8). Two major dust lanes lead into the central region. One of them comes in from the northwest, following the long tidal tail at larger radii. The other dust lane intersects the nuclear region from the north, cutting a bright ridge of emission regions into two parts. Hα emission is associated with the bright ridge of emission regions seen in the $V$ and $I$ images, and also with another emission patch across the dust lane coming in from the northwest. The emission ridge has $V-I$ colors around 1.0, but in the surrounding dusty area the $V-I$ colors are as red as 2. The southwestern emission region across the dust lane from the emission ridge has a blue $V-I$ color of 0.5. The nuclear spectrum of NGC 6621 has been classified to be of starburst type (Veilleux et al. 1995). The ground-based near-infrared data of Bushouse & Werner (1990) show that the nucleus likely lies near the

ridge of bright emission seen in our optical images, but it is not possible to constrain the true nuclear location from these images.

NGC 6622 has a well-defined nucleus and either a strong stellar bar, or a close to edge-on orientation to the line-of-sight (Fig. 9). The $J$-band infrared image of Bushouse & Werner (1990) shows that the outer isophotes are not too far from being circular, making it unlikely that this is an edge-on galaxy. There is an obvious dust lane on the northern and northeastern side of the galaxy, most likely signifying perturbations caused by NGC 6621. There is practically no Hα emission associated with NGC 6622, suggesting that it is an early Hubble-type galaxy. The nucleus and the bar have red $V-I$ colors up to 2.3. The typical color in the remainder of the disk is 1.3. There is a star forming region in the area between NGC 6621 and NGC 6622 which has a blue $V-I$ color with typical values around 0.8 (near the upper right edge of Figure 9).
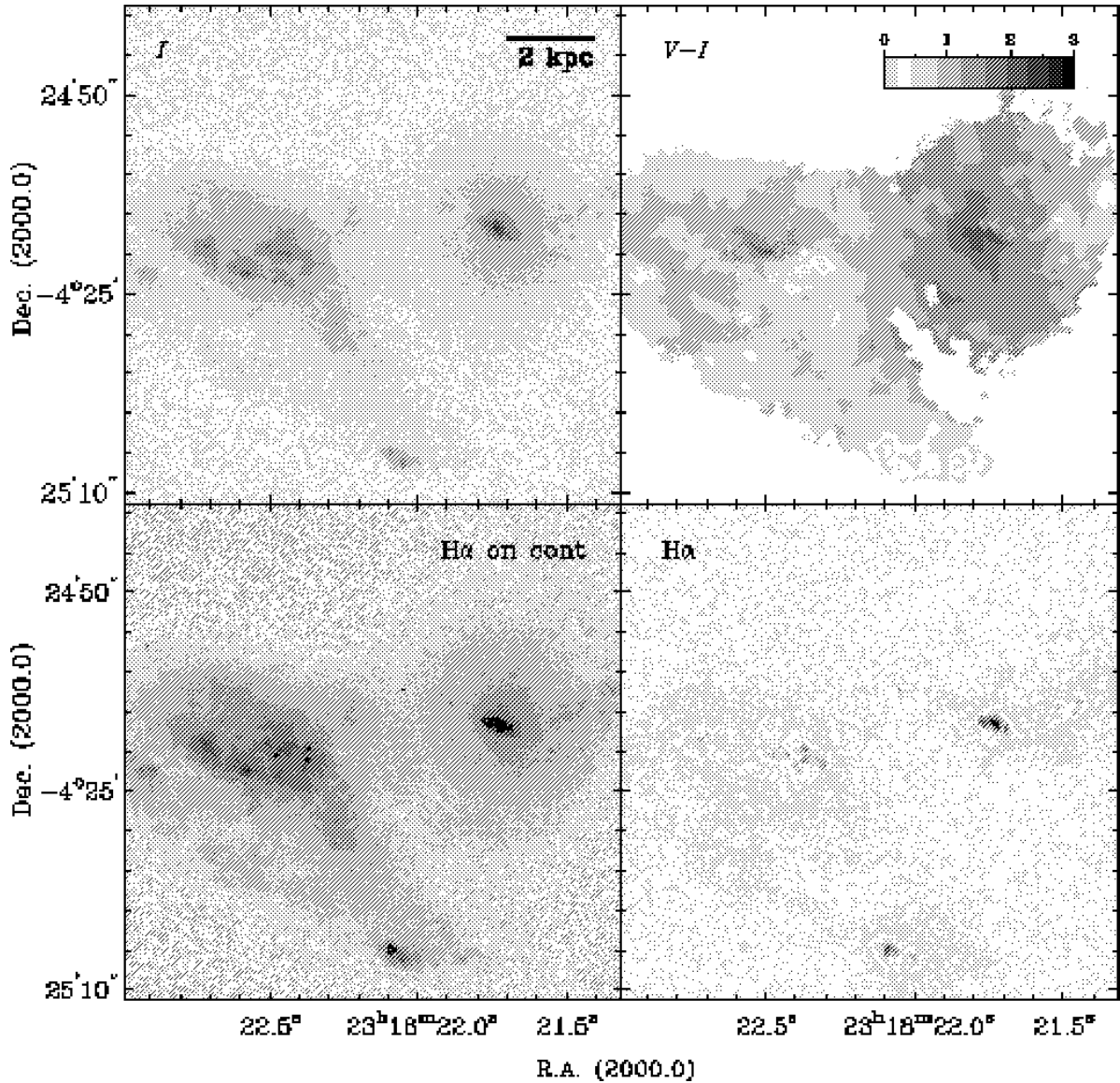
FIG. 6.— NGC 7592, as in Figure 2. The H$\alpha$ contour levels in the lower left image are at (10%, 30%, 50%) of $1.2\times10^{-15}$ ergs s$^{-1}$ cm$^{-2}$ per pixel.

### 3.6. NGC 3509

The second-most distant galaxy of this sample, NGC 3509, falls in the middle of the Toomre Sequence. The sketch of this system by Toomre (1977) suggests that he envisioned a large tail curving to the northwest and a shorter tail extending to the southwest. Deep ground-based CCD imagery obtained by one of us (JEH) suggests that the southeastern feature is not a tail, but rather the bright ridge of an inclined disk. There is a very bright rectangular-shaped feature at the head of the southeastern feature, directly south of a central bulge (see also Arp 1966), which may have been interpreted as the bulge of the second system. Our HST/WFPC2 broad-band imagery shows that this region resolves into a number of bright, blue stellar associations (Figure 10), and we believe it is much more likely to be a collection of bright star forming regions within the perturbed disk than the nucleus of a second system. The extremely blue colors of this region ($V - I$ colors around 0.5; the tip of this region is seen at

the bottom center of Figure 10) are in spectacular contrast to the rest of the galaxy (typical $V - I$ values from 1.1 to 1.4), and indicate active star formation.

In our images we can clearly identify a single relatively undisturbed nucleus, surrounded by a swirl of dust lanes (center of Figure 10). The H$\alpha$ image reveals a peculiar double-peaked H$\alpha$ structure straddling the nucleus in an orientation which is perpendicular to the main body of the nuclear region. H$\alpha$ emission, indicating ongoing star formation, is also seen in the blue region south of the nucleus.

In the absence of an obvious second tidal tail in the ground-based imagery, we find little evidence that NGC 3509 is the obvious result of a major disk-disk merger. It may instead be the result of a minor merger, or an ongoing interaction with a smaller companion. In support of the minor merger hypothesis, we note the appearance of a roughly circular diffuse red concentration just to the north of the nucleus ($12'' \sim 6$ kpc; see Fig. 1, just off of the PC chip) which could be the remains of a smaller
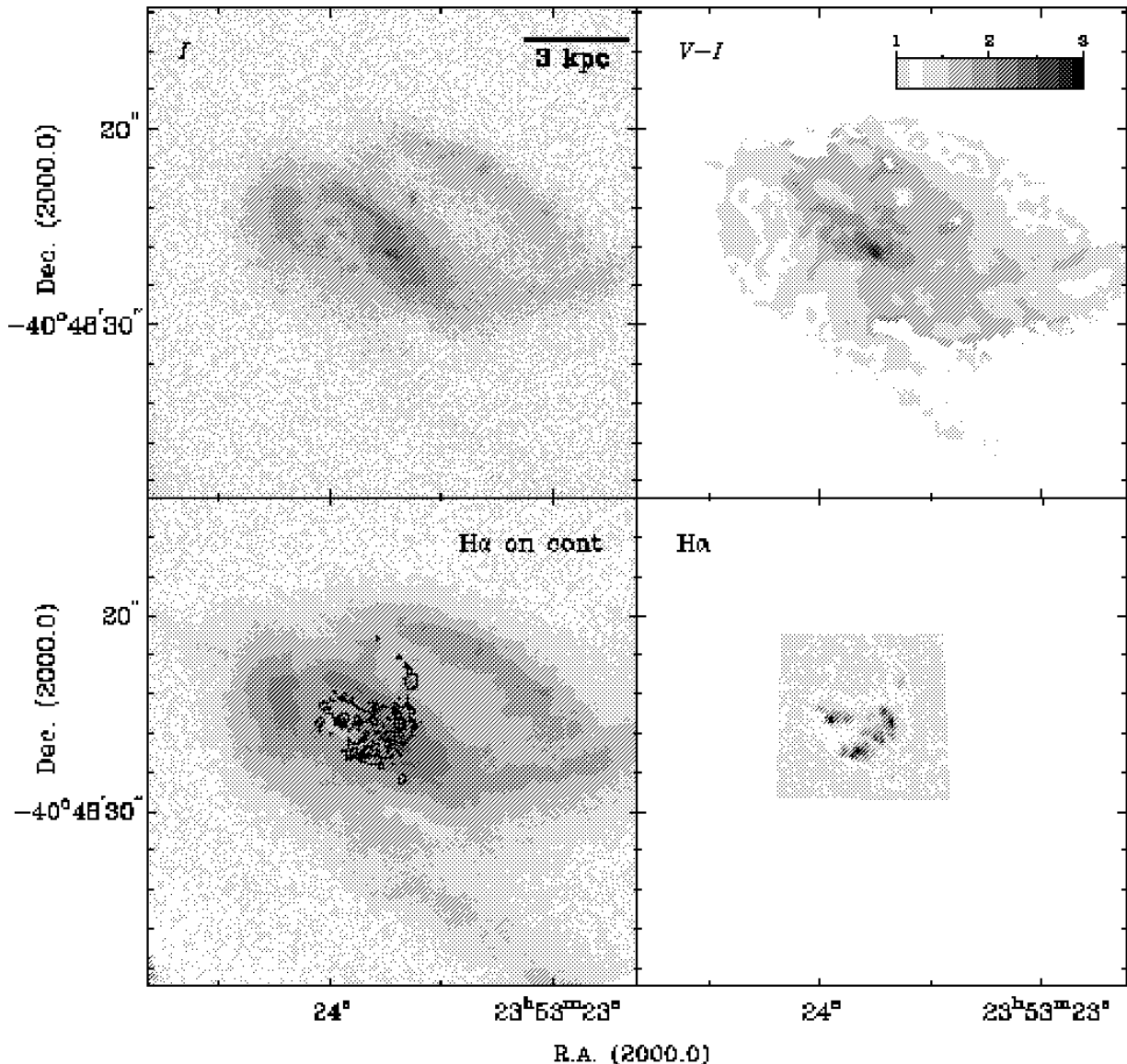
FIG. 7.— NGC 7764A, as in Figure 2. The Hα contour levels in the lower left image are at (10%, 30%, 50%) of $2.4 \times 10^{-16}$ ergs s$^{-1}$ cm$^{-2}$ per pixel.

galaxy. In support of the interaction hypothesis, on a deep R-band CCD image taken by one of us (JEH) we note the presence of a compact object lying $\sim 2'$ towards southeast, along the minor axis of this system. This possible companion also has faint low surface brightness features pointing both toward and away from NGC 3509.

### 3.7. NGC 520

The southeastern component of NGC 520 is hidden behind a prominent and intricate dust lane (Figure 11). This dust is likely associated with the dense edge-on molecular disk imaged in CO (1–0) by Sanders et al. (1988b) and Yun & Hibbard (2001). Adopting standard conversion factors, the observed peak CO flux density suggests that the nucleus of NGC 520 is hidden beneath $A_V \sim$ 300 magnitudes of extinction. It is thus not surprising that the position of the primary nucleus is impossible to determine from our data. High-resolution future NICMOS observations may point out where this nucleus lies, but based on

earlier ground-based near-infrared images (e.g., Bushouse & Stanford 1992; Kotilainen et al. 2001) the nucleus likely lies in the center of the heaviest dust absorption. Radio continuum images (e.g., Carral, Turner, & Ho 1990) show a disk-like morphology coincident with the CO disk, suggesting on-going star formation within the central molecular disk. Practically no Hα emission is seen in our Hα image at the position of the primary nucleus. Red $V - I$ colors are seen along most of the primary nucleus. However, at the location of the most dust-affected regions, as seen in the $I$ image, we see relatively blue colors of 0.8 in the color index image. Again, as in the case of NGC 4676A, we interpret this as scattering of emission from young stars, hinted at in the $V$-band image (not shown here).

The secondary, northwestern nucleus (Fig. 12) comes presumably from an earlier Hubble-type disk galaxy that is now embedded within an extended atomic gas disk associated with the primary galaxy (Hibbard & van Gorkom 1996). The secondary nucleus is very well defined, al-
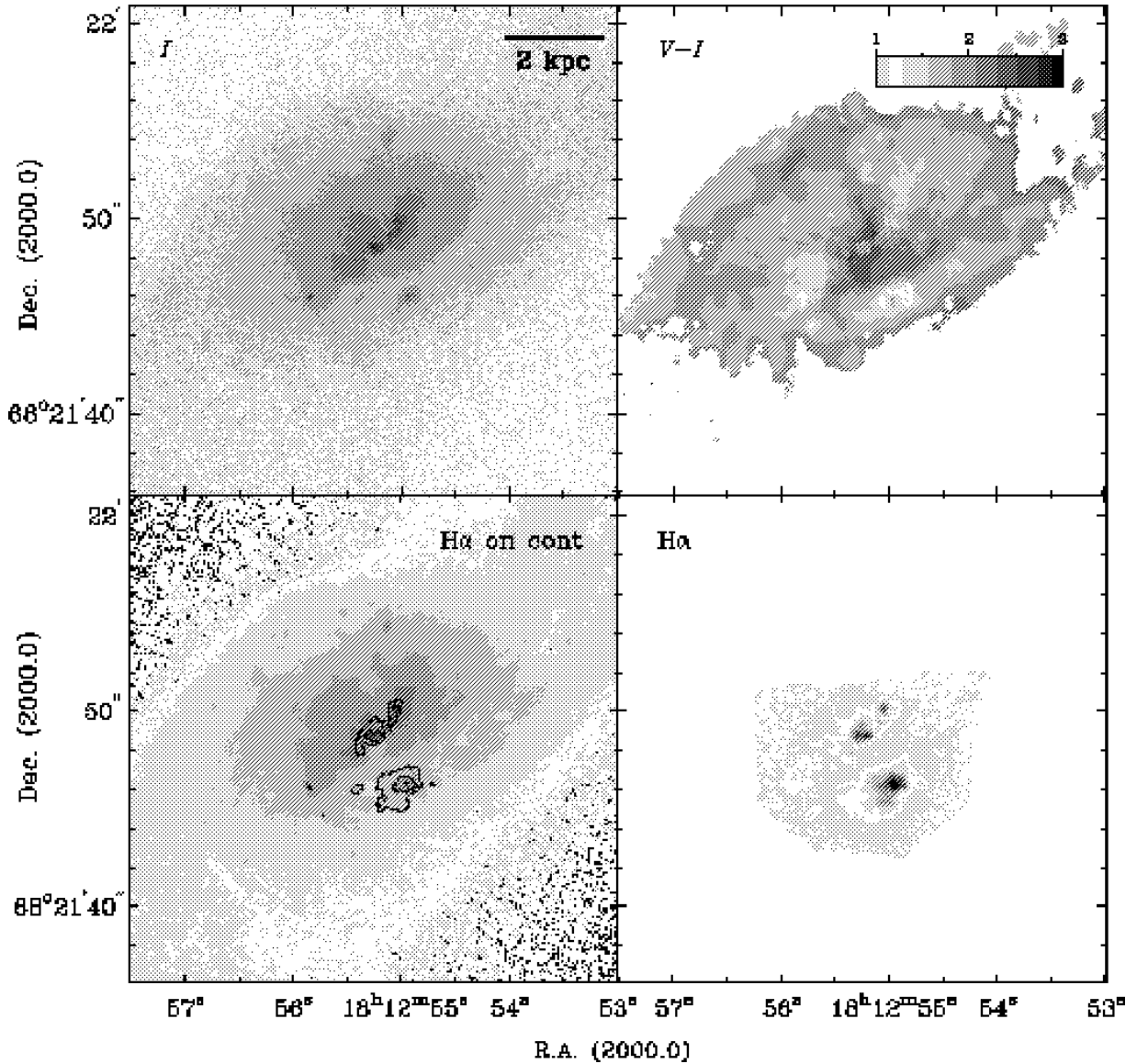
FIG. 8.— NGC 6621, as in Figure 2. The Hα contour levels in the lower left image are at (5%, 20%, 90%) of $1.9 \times 10^{-15}$ ergs s$^{-1}$ cm$^{-2}$ per pixel.

though its surrounding disk seems to have been mostly disrupted in the merger, and probably contributes now to the extended optical tails. The only significant Hα emission near the secondary nucleus is in clumps within 1″ (150 pc), and displaced to the northwest. The secondary nucleus appears to have a bluish color, with $V-I$ of 0.6. This nucleus is observed to be in a post-starburst phase (Stanford & Balcells 1990, 1991; Bernlöhr 1993). The $V-I$ color towards the northwest of the nucleus has bluish values around 0.8, but dust reddens the color to 1.2 at about 3″ (450 pc) southeast of the nucleus.

### 3.8. *NGC 2623*

Consistent with its classification as a fairly advanced merger system, only one galaxy body is evident in NGC 2623 (Fig. 13). Again, based on the high spatial resolution optical *HST* images it is impossible to tell the exact location of the nucleus or nuclei. A comparison to the *JHK* NICMOS images published by Scoville et al.

(2000) suggests that the position of the brightest optical peak in the center of the main body of NGC 2623 is the true position of the nucleus, near J2000.0 coordinates of R.A.=$8^h38^m24^s.1$ and Dec.=$25°45'16''.6$. This nucleus is classified as a LINER by Dahari (1985) and Vacci, Alonso-Herrero, & Rieke (1998). Dust surrounds the nucleus mostly on the southeastern, northern, and northwestern sides, although numerous dust lanes criss-cross the whole nuclear region (see Fig. 13).

A study by Joy & Harvey (1987) confirms the coalescence of two galaxies. Based on their near-infrared observations, they conclude that the merger is complete, because only one nucleus is visible (which is surrounded by a single, symmetric nuclear region). This impression is confirmed by CO observations, which reveal a single centrally concentrated compact molecular disk with simple rotational kinematics (Bryant & Scoville 1999). There are also numerous young star clusters scattered around the main body and the surrounding shreds.
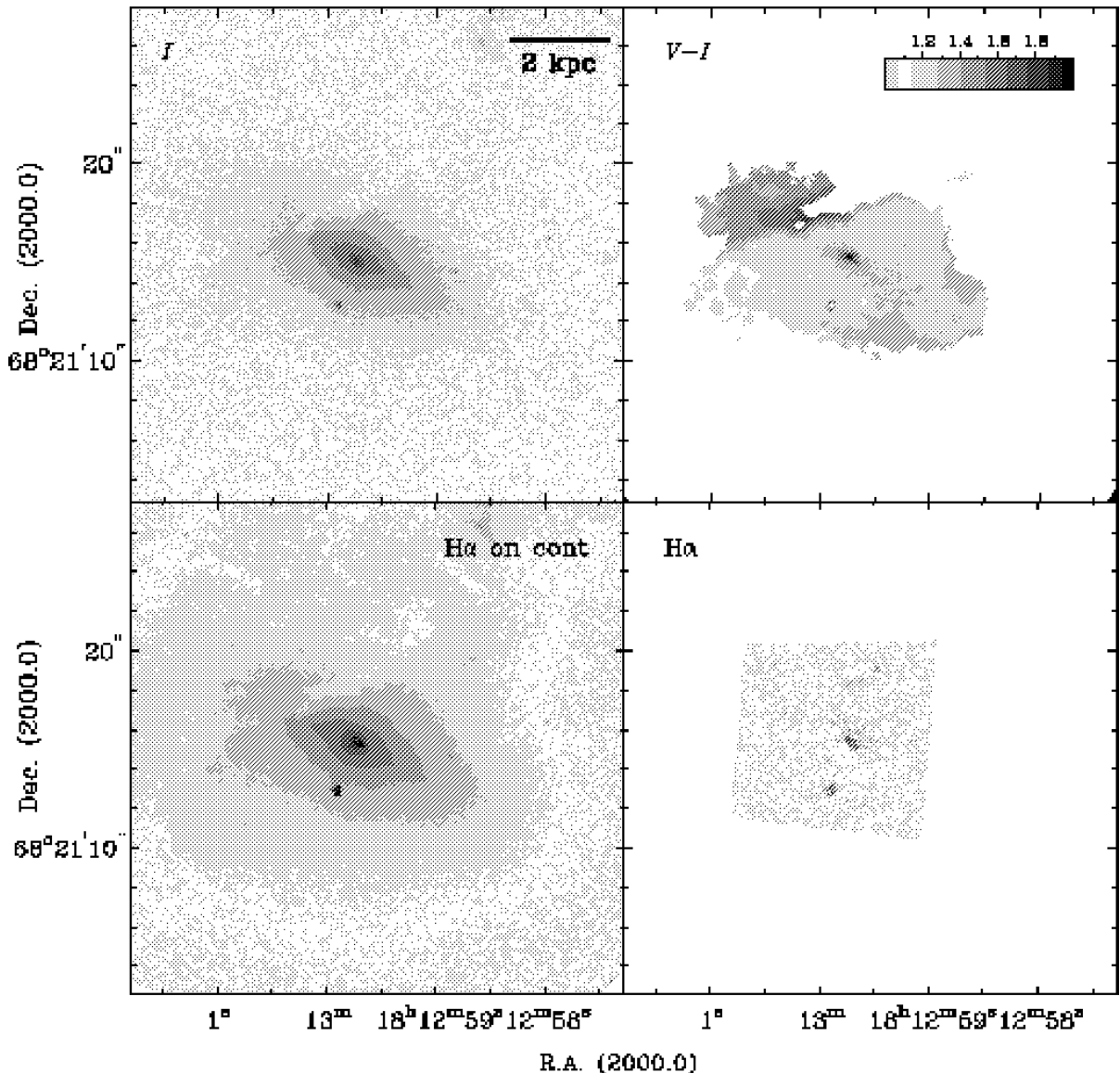
FIG. 9.— NGC 6622, as in Figure 2. The Hα contour level in the lower left image is at 50% of $7.3 \times 10^{-17}$ ergs s$^{-1}$ cm$^{-2}$ per pixel.

Most of the Hα emission comes from a disk around the nuclear position and from a location north of the nucleus, but also from a position in the dust patch southeast of the nucleus. The nucleus has a very red $V - I$ color at 2.5, consistent with the reddish near-infrared colors found for the nucleus by Scoville et al. (2000). The red near-infrared $H - K$ color, together with a relatively large CO absorption index value (Ridgway et al. 1994) suggest that there has been a recent starburst in the nuclear region. The red colors continue for about $2''$ (720 pc) to the north and northwest. The main body of NGC 2623 has $V - I$ colors close to 1.0 or just below it.

### 3.9. NGC 3256

Our optical $HST$ images show one obvious nucleus located in the center of Figure 14 (see also Zepf et al. 1999). This nucleus is surrounded by a relatively symmetric spiral morphology. Near-infrared, radio continuum, and X-ray observations (e.g., Norris & Forbes 1995; Kotilainen et al. 1996; Lira et al. 2002) have discovered a second nucleus

about $5''$ (885 pc) south of the primary nucleus (marked with an "X" in Fig. 14), presumably hidden beneath the dark (red) dust feature directly south of the primary nucleus in the $V - I$ image of Fig. 14 (see also English et al. 2003). We do not see an optical source at the position of the second near-infrared, radio, and X-ray source. Our data therefore do not shed any new light on the nature of this source. Neither nucleus shows any evidence of being active. Studying the question of how many nuclei exist in this system (even three nuclei have been suggested by Lipari et al. 2000), would benefit from a detailed dynamical simulation of this merger system. The measurements for NGC 3256 in this paper refer only to the one nucleus we see in our WFPC2 images.

Archival NICMOS near-infrared images suggest that the position of the primary nucleus is close to the location of the brightest emission in our F814W image (Lipari et al. 2000). However, the optical $HST$ images alone only show that this position is part of a ring-like structure, and there is nothing noticeably different about this location other
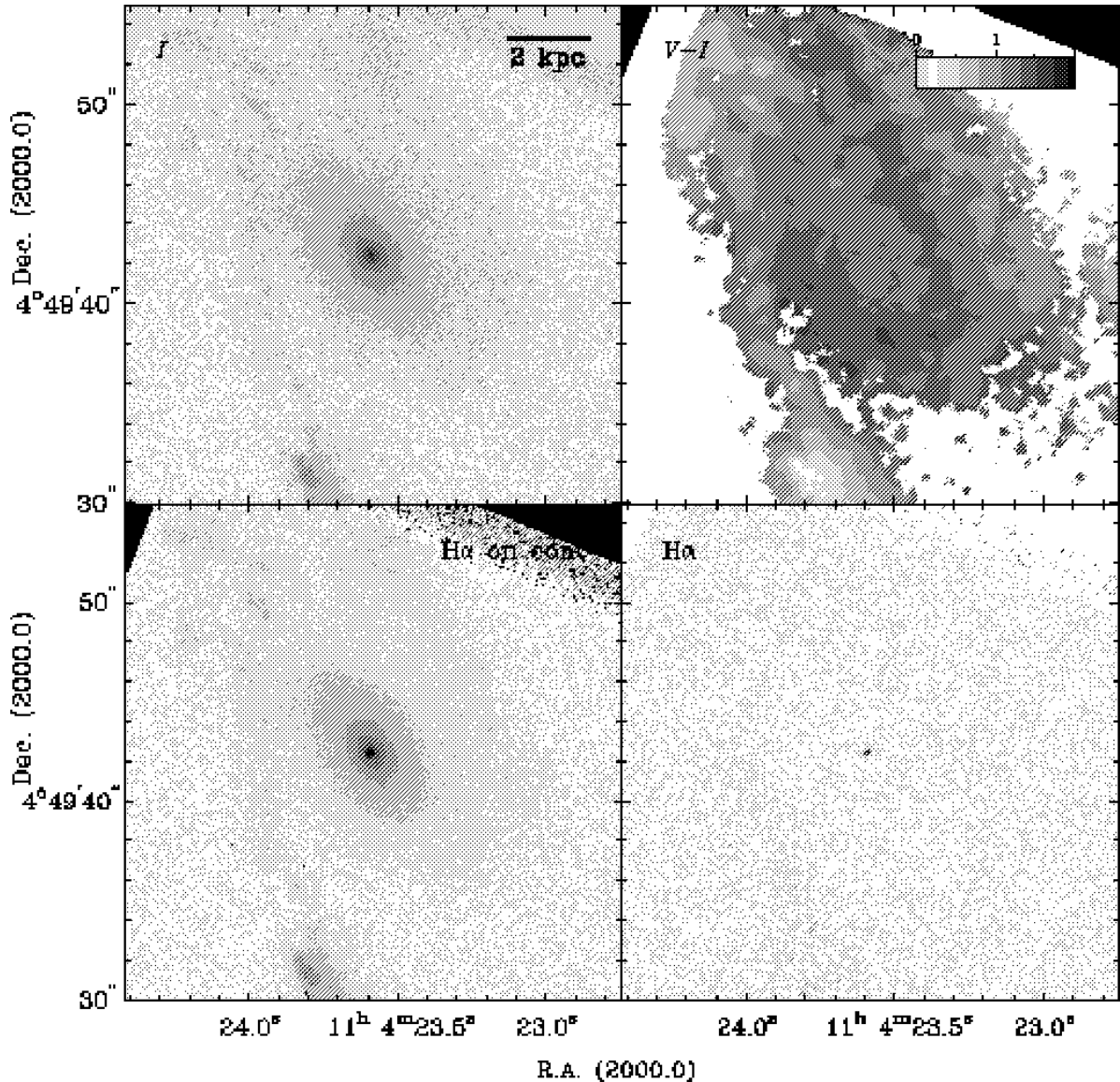
FIG. 10.— NGC 3509, as in Figure 2. The Hα contour level in the lower left image is at 20% of $2.5 \times 10^{-16}$ ergs s$^{-1}$ cm$^{-2}$ per pixel.

than that it is the brightest clump in the image. Other bright regions are likely to be young star clusters or globular clusters, as reported by Zepf et al. (1999).

The Hα emission is extended and follows the spiral structure, but the brightest emission occurs at the position of the primary nucleus. Most previous studies regard this nucleus to be of starburst type, although Véron–Cetty & Véron (1986) were unable to resolve its true nature. While the primary nucleus has a blue $V - I$ color near 0.7, the dusty region covering the secondary nucleus to the south of the primary nucleus has a $V - I$ color of 2.5 or redder. In contrast, the spiral arms visible in the $V$ and $I$ images have a blue $V - I$ color between 0.5 and 1.0.

### 3.10. NGC 3921

Only one nucleus is visible in NGC 3921 (Figure 15). This galaxy is a post-merger system that has developed an elliptical-like central region (see, e.g., Schweizer 1996; Schweizer et al. 1996; Hibbard & Yun 1999), although numerous dust lanes still criss-cross this area (see Fig. 15).

The evidence for a recent merger can be seen in the outer region where tails and plumes prevail (Hibbard & van Gorkom 1996). Several compact open star clusters or globular clusters can also be seen in the HST optical images kindly provided by B. Whitmore (see also Schweizer et al. 1996).

The Hα emission is centered in a disk around the nucleus, but extends to larger radii. The nucleus is classified as a LINER by Stauffer (1982a,b) and Dahari (1985). It lies in a location where the $V - I$ color gradient is very steep as seen in the $V - I$ image, but the nucleus itself has normal values of $V - I$ around 1.1. To the southwest of the nucleus the $V - I$ color increases to $\sim 1.8$ at about 0″.5 (190 pc) distance from the nucleus, and then decreases and stays around 1.1–1.2 on that side of the galaxy. To the northeast, the $V - I$ color decreases to values as low as 0.7 at about 0″.5 from the nucleus, then stays around 0.9 for another 1″.5 (570 pc). Dust extinction is at least partly responsible for this effect. Schweizer (1996) noticed that the nucleus lies substantially off-centered from the outer
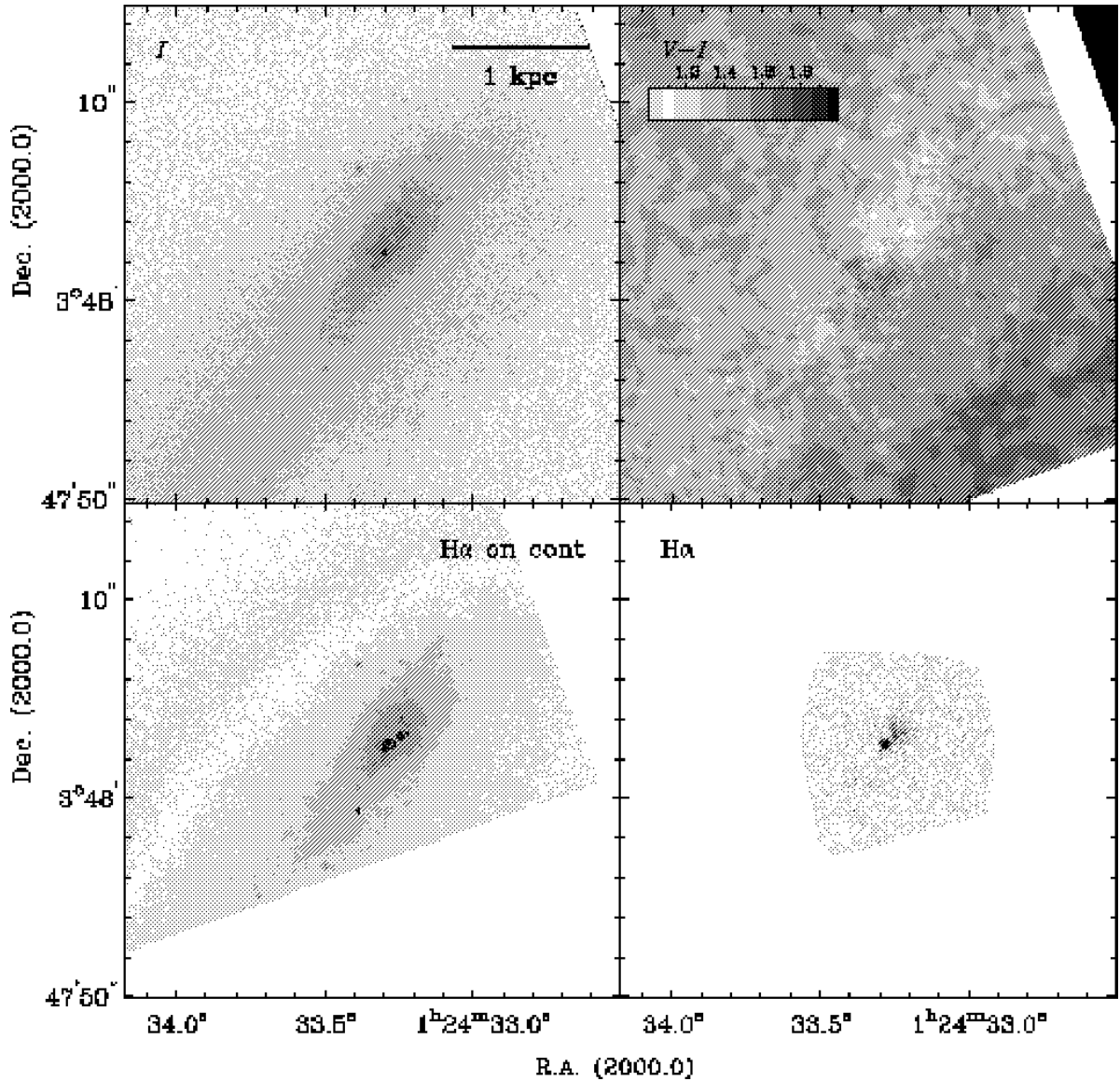
Fɪɢ. 11.— NGC 520 Nuc 1. Left: $I$ image. Right: $V - I$ image. The Hα emission around the nucleus is not shown as it is not significantly detected above the noise of the image.

stellar isophotes of the main body.

### 3.11. NGC 7252 ("Atoms–for–Peace" Galaxy)

We use the $HST$ $V$ and $I$ images from Miller et al. (1997) to study the most advanced merger in the Toomre Sequence. The remnant from the merger is probably between 0.5 and 1 Gyrs old (Schweizer 1982; Hibbard & Mihos 1995). It has a single nucleus and is characterized by a $r^{1/4}$ profile typical of elliptical galaxies (Schweizer 1982; Miller et al. 1997; Hibbard & Yun 1999). It was quite a surprise, therefore, when $HST$ revealed a central spiral disk (Miller et al. 1997 and Fig. 16). The disk extends to a radius of about $6''$ (1.8 kpc), and is therefore coincident with the molecular disk imaged by Wang et al. (1992). Our new $HST$ Hα image of this galaxy shows the disk to be actively forming stars, while the $V - I$ color map shows dust to be intertwined between the arms. In light of the results from recent hydrodynamical simulations (Barnes 2002), and the observation of tidal gas streaming back into the central regions of this remnant from the tidal tails (Hibbard et al. 1994; Hibbard & Mihos 1995), it seems likely that this central disk structure results from the re-accretion of tidally raised gas into the now-relaxed central potential.

The nucleus appears resolved, and is very bright, as we show in Section 4. Hα emission largely follows the spiral arms, although there appears to be a central Hα source as well. However, our continuum subtraction, unfortunately, is uncertain in this area due to an optically very bright nucleus. Similarly, the central $V - I$ color is difficult to determine reliably due to the same problem, but the color there appears to be close to 1.3, whereas the surrounding spirals have $V - I$ colors as blue as 0.5.

Recent X-ray observations with ASCA revealed X-ray emission that can be described by a two-component model (Awaki et al. 2002), with soft emission (kT = 0.72 keV), and a hard component (kT > 5.1 keV). The hard component might indicate the existence of nuclear activity or even an intermediate mass black hole.

### 4. CHANGE IN PHOTOMETRIC PROPERTIES WITH MERGER STAGE

We performed aperture photometry of the Toomre Sequence galaxies to better understand the evolution of the nuclear region of merging galaxies. Because the isophotes in the nuclear region of merging galaxies are highly twisted, we did not attempt to fit ellipses and obtain radial surface brightness profiles. Instead we performed aperture photometry within circular apertures, with radii of 100 pc and 1 kpc. The lower value was dictated by the smallest resolvable physical scale in the most distant of our sample galaxies, whereas the upper value is somewhat arbitrary, but set because of our emphasis on the properties of the nuclear region. We have already characterized the morphology of the nuclear region at $HST$ resolution in the individual galaxies above. Here we only report on the bulk photometric nuclear properties of each identified merger component galaxy.

Visual inspection of the images quickly reveals that none of the galaxies in the sample possess an extremely bright, point-like active nucleus. Based on spectroscopic evidence, as cited in Section 3, the only mildly active nuclei are in NGC 7592A (Seyfert 2), NGC 4676 Nuc 1 and Nuc 2 (LINER), NGC 2623 (LINER), and NGC 3921 (LINER). It is difficult to assess what the exact contribution of the nucleus to the integrated luminosities is.

The photometric measurements, converted to luminosity densities, are presented in Figures 17–19. The "merger stage", plotted along the x-axis, refers to the original order of the sequence given by Toomre (1977), where 1 corresponds to NGC 4038/39 (the earliest merger stage) and 11 to NGC 7252 (the latest merger stage). The exact correspondence is given in the figure caption to Figure 17. Our observations do not suggest an obvious reordering of this sequence, although we are hampered by our inability to unambiguously identify all of the putative nuclei. Our tentative impression is that NGC 7764A (merger stage=4) may be interacting with the disturbed galaxy lying off of

FIG. 12.— NGC 520 Nuc 2, as in Figure 2. The Hα contour levels in the lower left image are at (20%, 90%) of 1.4×10$^{-16}$ ergs s$^{-1}$ cm$^{-2}$ per pixel.

our image, in which case it belongs near the beginning of the sequence. And NGC 3509 (merger stage=6) is not an obvious merger at all. However, we will await NIC-MOS observations of this sequence before reaching any firm conclusions on this matter. We note that none of our conclusions will be affected if these two systems move earlier along or off of the sequence.

Apart from the large scatter in Figure 17 we see that the three latest merger stage systems (NGC 3256, NGC 3921, and NGC 7252) have the highest intrinsic luminosity densities. This is true for both apertures that we used (100 pc and 1 kpc). The range of luminosity density within 100 pc corresponds to a factor of more than 300. To a large extent this reflects the varying dust extinction in the central region, but partly also the morphology of the nuclear region (well-defined nuclei are bright, whereas components with no clearly recognizable nucleus are faint). With only $V - I$ colors available it is difficult to make a meaningful estimate of dust extinction. But, for example, Figure 18

shows that in NGC 2623 the integrated $V - I$ color is very red within a 100 pc radius aperture, with a value around 2.2. Assuming that the true $V - I$ color is 1.4 (a more typical value seen in the same figure), would imply almost $A_V = 2$ mag of extinction with a typical extinction law of $A_\lambda \sim \lambda^{-1.85}$ (Landini et al. 1984). Since the extinction in the $K$-band is only one tenth of that in the $V$-band, our future NICMOS images offer some hope of revealing the true location of the nucleus.

While the $V - I$ colors for the 100 pc aperture attain values anywhere between 0.8 and 2.4, the majority of the nuclei have rather typical colors for the centers of spiral nuclei and elliptical galaxies, ranging from 1.2 to 1.5 (cf., e.g., Carollo et al. 1997). The presumably latest stage merger, NGC 7252, has colors even bluer than normal ellipticals. However, the morphology of the dust lanes we see in the images suggests that dust obscuration is likely to be significant in many systems of the Toomre Sequence.

The Hα + [N II] luminosities (Figure 19) show a
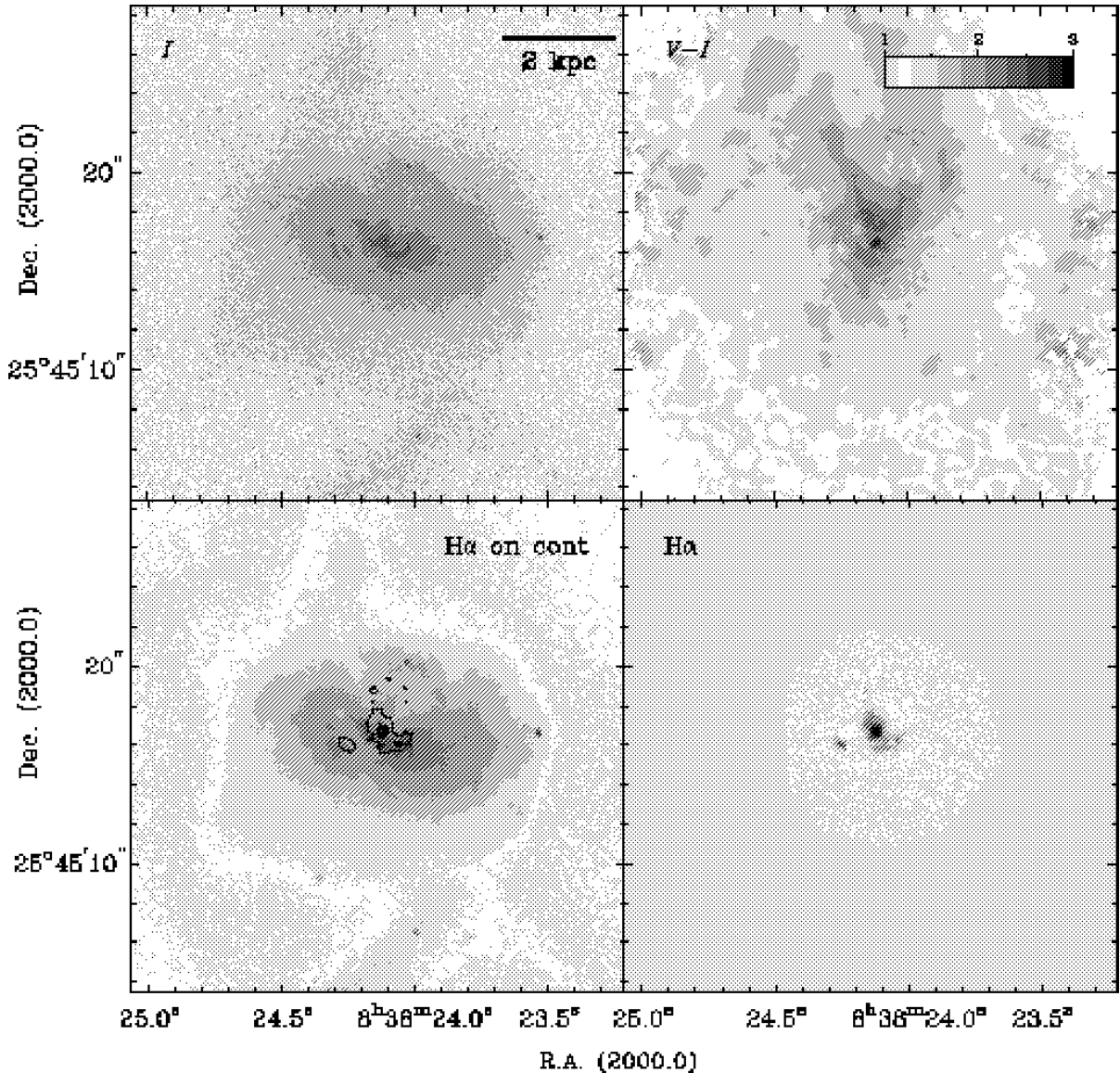
FIG. 13.— NGC 2623, as in Figure 2. The Hα contour levels in the lower left image are at (10%, 50%, 80%, 90%) of $3.3 \times 10^{-16}$ ergs s$^{-1}$ cm$^{-2}$ per pixel.

marginal trend of increasing luminosities towards the late-stage mergers, most obviously in the largest 1 kpc aperture. However, the scatter is large, and based on the sample of 15 nuclei it is impossible to establish any definite trends.

Since mergers are expected to bring material into the center of galaxies and generate star formation there, we also study the nuclear concentration of light and line emission along the merging sequence. We measure the nuclear concentration quantitatively by taking the ratio of the luminosities within 100 pc to that within 1 kpc, for both the I-band (Figure 20) and the line emission (Figure 21). We discuss the meaning of these ratios briefly in the following section.

## 5. DISCUSSION AND SUMMARY

The nuclear morphologies and central concentration are expected to be strongly affected by the timing and intensity of induced inflows and star formation during the

merger. Numerical models of interacting galaxies have illustrated one mechanism by which interactions trigger these inflows and nuclear activity. Shortly after the galaxies first collide, the self-gravity of each disk amplifies the collisional perturbation into a growing $m = 2$ mode (Noguchi 1988; Barnes & Hernquist 1991; Mihos & Hernquist 1996). Depending on the structural properties of each galaxy, this mode can take the form of a strong bar, prominent spiral arms, or a pronounced oval distortion (Mihos & Hernquist 1996; Mihos et al. 1997). These non-axisymmetric structures drive shocks in the interstellar medium of the galaxies, leading to a spatial offset between the gaseous and stellar components which robs the gas of angular momentum, and can drive it inwards well before the galaxies ultimately merge (Barnes & Hernquist 1991; Hernquist & Mihos 1995; Mihos & Hernquist 1996). The onset, strength, and duration of starbursts in interacting pairs can vary widely, depending on the properties of the host galaxies. Ultimately, however, any dynamical
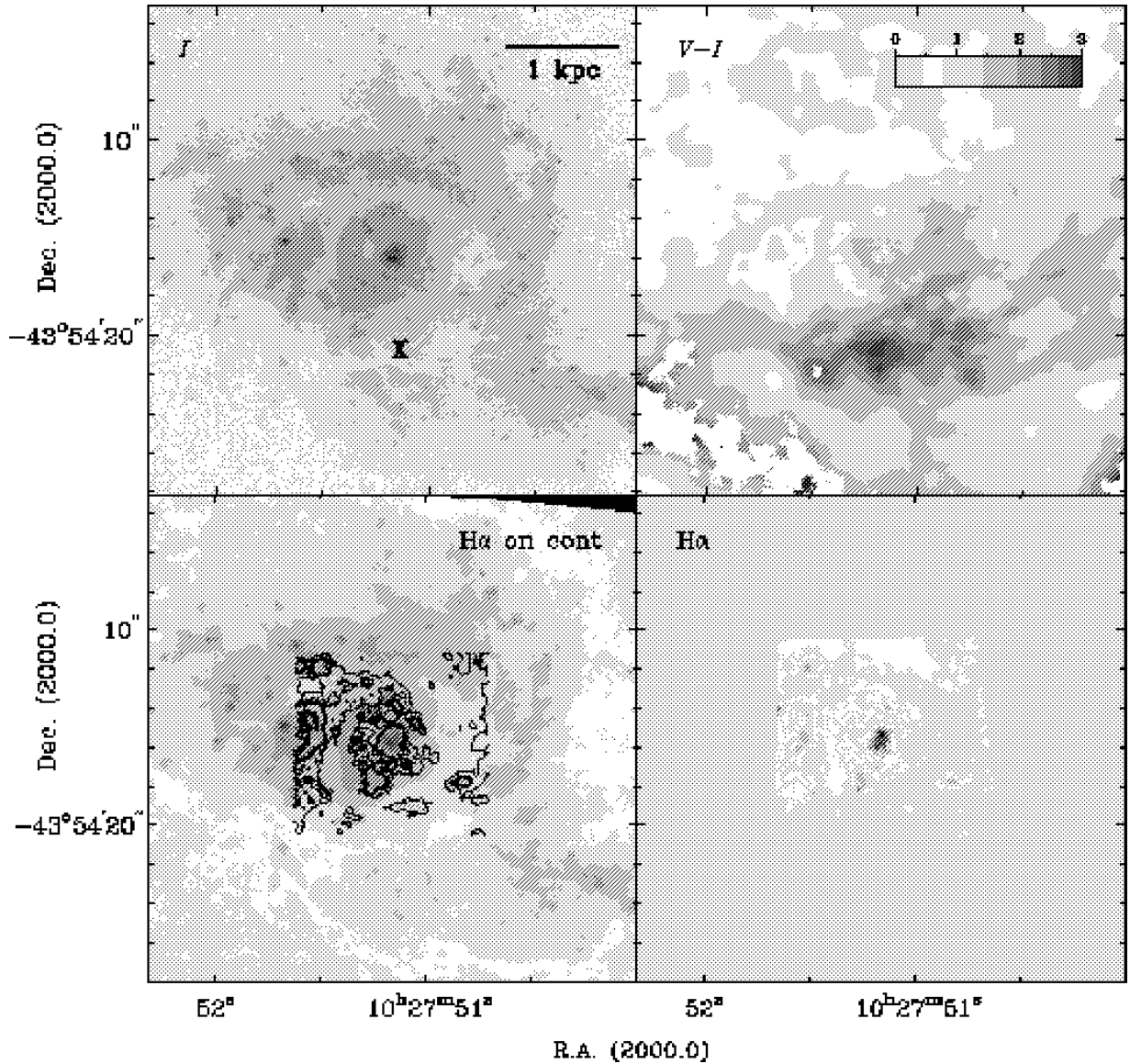
FIG. 14.— NGC 3256, as in Figure 2. The location of the putative second nucleus is marked with an "X" in the upper left panel. The Hα contour levels in the lower left image are at (10%, 50%, 80%, 90%, 95%, 98%) of $3.5 \times 10^{-16}$ ergs s$^{-1}$ cm$^{-2}$ per pixel.

stability provided by the presence of a central bulge or diminished disk surface density will be overwhelmed by the strong gravitational torques and dissipative shocks during the final merging of the pair, at which point gaseous inflow and central activity should be ubiquitous. Once the coalescence of the galaxies is complete, the gravitational potential settles down and gas can resettle into nuclear and/or spatially extended disks, supporting an extended period of relatively quiescent star formation.

Based on these kinds of models, we might expect to see an evolutionary trend for the nuclear properties of the Toomre Sequence, from quiescent star formation in the early stages of the sequence to strong nuclear activity in the late stages. However, we see little evidence for such trends in the morphology, luminosity density, or colors of the stellar component, or in the morphology or intensity of the ionized gas emission, apart possibly from the fact that the latest-stage systems have some of the highest broadband luminosity densities and hints of starbursting central

gaseous disk structures. This last suggestion is further strengthened by the trend towards bluer colors among the three latest-stage merger systems in Figure 18. A trend towards bluer colors was also seen in a study of merger remnants by van der Marel & Zurek (2000). Furthermore, the latest-stage merger systems have some of the highest nuclear Hα luminosities (Figure 19) and possess some of the largest concentrations of light in the central region (Figure 20). Such a concentration is also seen to a certain extent in the Hα+[N II] emission (Figure 21).
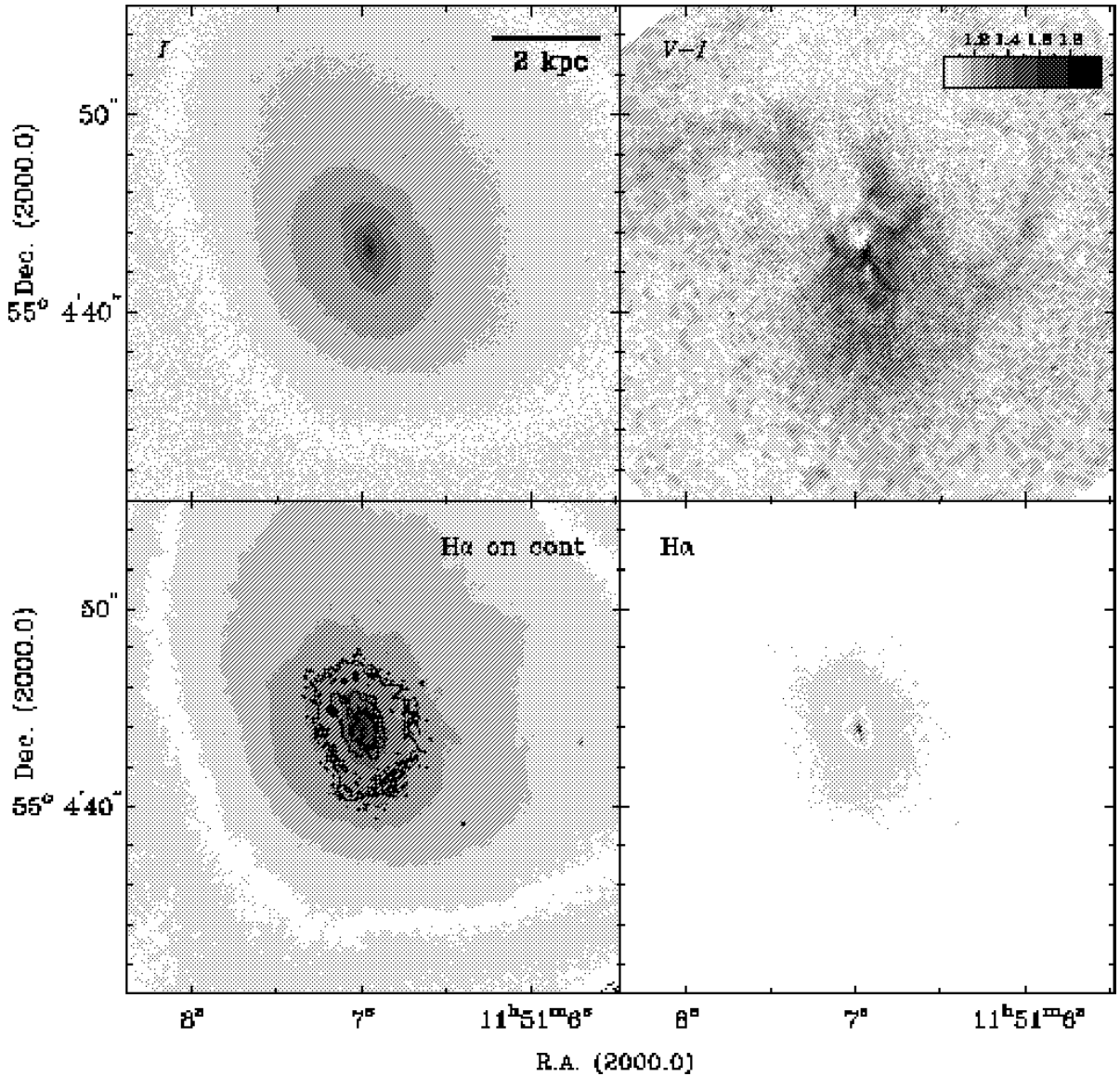
FIG. 15.— NGC 3921, as in Figure 2. The Hα contour levels in the lower left image are at (10%, 30%, 50%, 70%, 90%) of $1.9 \times 10^{-16}$ ergs s$^{-1}$ cm$^{-2}$ per pixel.
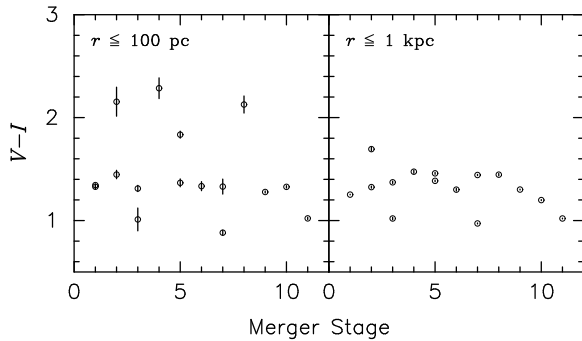


FIG. 18.— Integrated $V - I$ color indices within the circular apertures cited within the frames, as a function of the merger stage. The merger stage is defined as before in Figure 17. The error bars are based on the combined errors in the $V$- and $I$-band aperture magnitudes, estimated using the standard propagation of error formulas.

Are our observations of the Toomre nuclei consistent with the broad picture of interaction-induced nuclear activity in galaxies evidenced in numerical simulations? In a broad sense, yes, although this consistency is mainly due to the variety of dynamical responses available to interacting systems. The late stage mergers seem to have settled down, showing evidence for nuclear emission-line disks (NGC 2623, NGC 3256, NGC 3921, and NGC 7252), more concentrated luminosity profiles and a trend towards bluer colors. Toomre Sequence objects at earlier stages show very diverse properties, with no clear trends along the sequence. However, selecting a merging sequence based largely on the large-scale morphology of the tidal tails biases the sample towards a specific type of interaction – prograde interactions between disk galaxies – but not a specific type of disk galaxy. The galaxies which make up the Toomre Sequence likely possess a variety of structural properties so that there is no one-to-one correspondence between observed merger stage and nuclear morphology and activity. Put differently, the Toomre Sequence is *not* a true evolutionary sequence on anything but the largest scales. Instead, it is composed of a variety of galaxies pro-
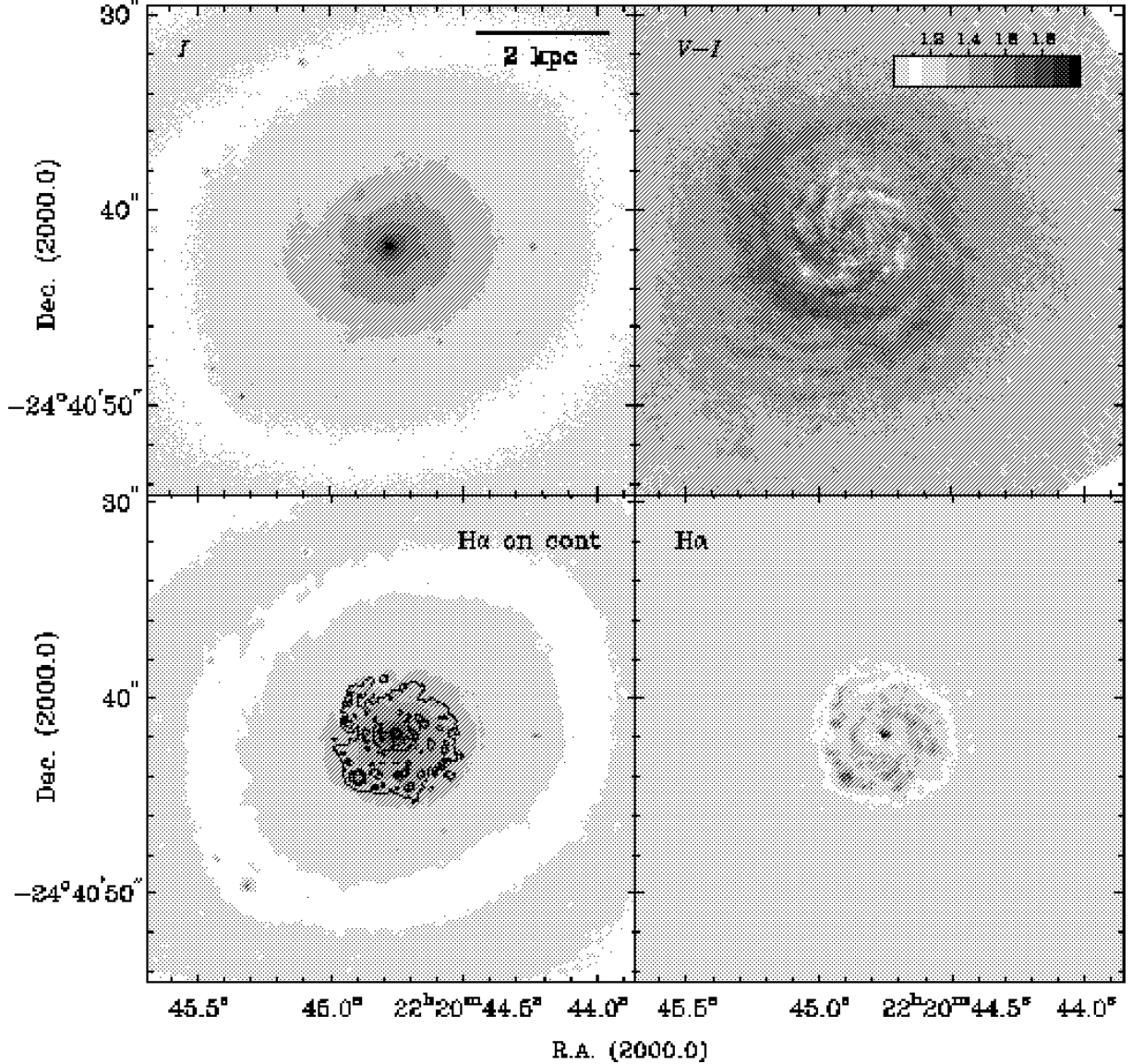
FIG. 16.— NGC 7252, as in Figure 2. The Hα contour levels in the lower left image are at (10%, 30%, 50%) of $7.2\times10^{-16}$ ergs s$^{-1}$ cm$^{-2}$ per pixel.

gressing down varied paths of interaction-driven activity. Expecting to discern a clear trend in nuclear properties is likely a naive hope.
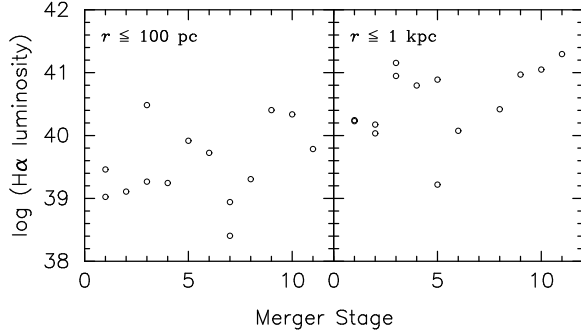


FIG. 19.— Integrated Hα+[N II] luminosities in units of ergs sec$^{-1}$ within the circular apertures as cited within the frames, as a function of the merger stage. The merger stage is defined as before in Figure 17. It was impossible to measure the flux within 1 kpc reliably for NGC 520 Nuc 2 (merger stage 7), since the galaxy was so close to the edge of the chip. Therefore, no 1 kpc luminosity is plotted here and in Figure 21. Uncertainties in the fluxes are no better than 50%.

Aside from the variety of physical conditions sampled by the Toomre nuclei, searching for trends along the Toomre Sequence is also hampered by a number of observational concerns. First, the orientation of the galaxies with respect to the line-of-sight and to the orbital plane of the merger complicates the interpretation of the images. Second, extinction has a large effect on the observed morphologies, colors, and luminosities, as shown in Section 4 (e.g., NGC 520 Nuc 1 and NGC 4676 Nuc 1). In this context, we hope to improve upon the interpretation of the galaxy morphologies along the sequence through an analysis of NICMOS images of the entire Toomre Sequence.
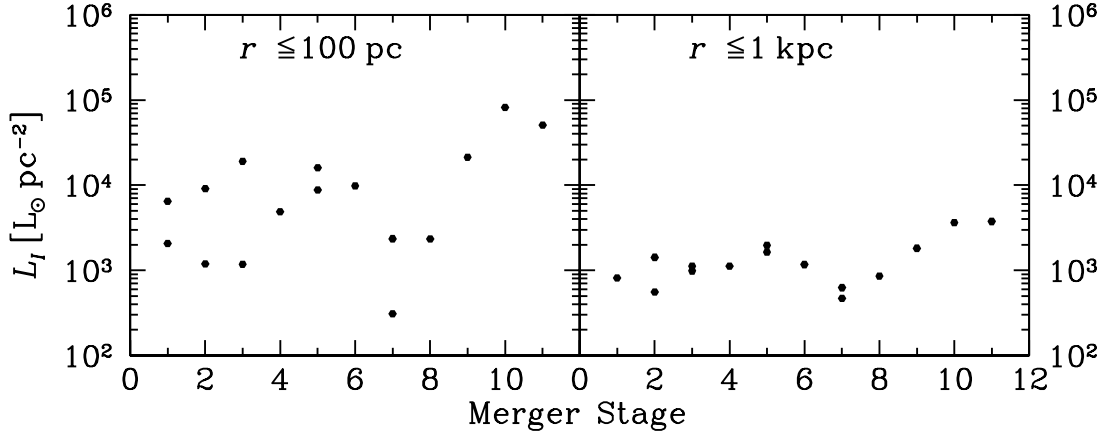
FIG. 17.— Circular $I$-band aperture photometry centered on the putative nucleus in each of the merging galaxies of the Toomre Sequence. The horizontal axis represents the sequence as originally conceived by Toomre (1977). The merging stage numbers correspond to the individual galaxies as follows: 1: NGC 4038/39; 2: NGC 4676; 3: NGC 7592; 4: NGC 7764A; 5: NGC 6621/22; 6: NGC 3509; 7: NGC 520; 8: NGC 2623; 9: NGC 3256; 10: NGC 3921; 11: NGC 7252. The two-dimensional projected luminosity density is presented on the vertical axis, within apertures specified within the frame. Left, within a 100 pc radius aperture, right, within a 1 kpc radius aperture. The luminosity densities have not been corrected for extinction. Uncertainties in the plotted values are smaller than the symbol size.

These images will suffer from much less extinction, and should also reveal the isophotes of the stellar population more clearly, thereby helping us in assessing the inclination of the merger components. The optical images shown here clearly demonstrate that dust in merging galaxies, even on small scales resolved by the *HST*, is not patchy enough to enable the identification of the true nuclei in optical bands.

geometry, as well as the physical variety of galaxies involved in the Toomre Sequence. In subsequent papers we will combine our optical imaging with NICMOS imaging and STIS spectroscopy of the Toomre nuclei to give a detailed picture of the physical conditions in interacting and merging galaxies.
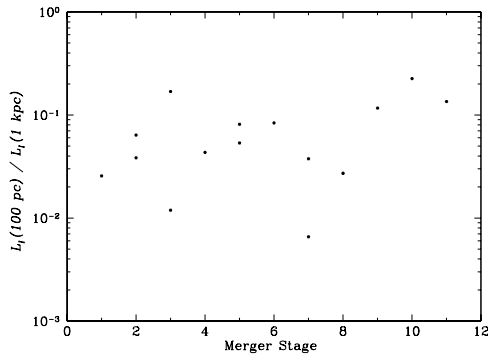


FIG. 20.— Ratio of the integrated $I$-band luminosity inside 100 pc to the integrated luminosity inside 1 kpc, plotted on a logarithmic scale, as a function of the merger stage.



FIG. 21.— Ratio of the integrated H$\alpha$+[N II] luminosity inside 100 pc to the integrated H$\alpha$+[N II] luminosity inside 1 kpc, as a function of the merger stage. Uncertainties in the fluxes are no better than 50%.

In summary, these high-resolution WFPC2 images of the Toomre Sequence have given us a detailed view of the nuclear regions of interacting and merging galaxies. We have characterized the broad-band and emission-line morphologies of each member of the sequence, and measured the colors and luminosity densities of the nuclei. We find little evidence for clear trends in nuclear properties along the merger sequence, other than a suggestive rise in the nuclear luminosity density in the most evolved members of the sequence. The lack of clear trends in nuclear properties is likely due both to the effects of obscuration and
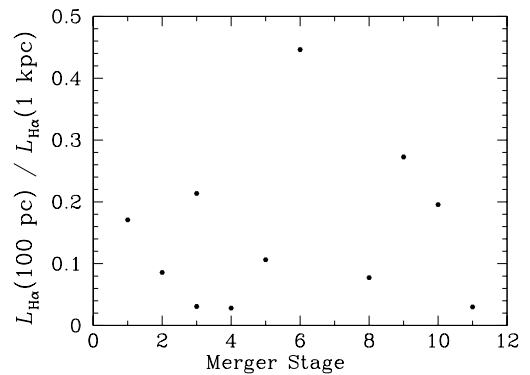
## REFERENCES

Arp, H. 1966, Atlas of Peculiar Galaxies, (Pasadena: California Institute of Technology)

Awaki, H., Matsumoto, H., & Tomida, H. 2002, ApJ, 567, 892

Bahcall, J. N., Kirhakos, S., & Schneider, D. P. 1995, ApJ, 450, 486

Barnes, J. E. 1988, ApJ, 331, 699

Barnes, J. E. 1998, in Saas-Fee Advanced Course No. 26, "Galaxies: Interactions and Induced Star Formation", ed. D. Friedli, L. Martinet & D. Pfenniger (Berlin: Springer–Verlag), 275

Barnes, J. E., 2002, MNRAS, 333, 481

Barnes, J. E., & Hernquist, L. 1991, ApJ, 370, L65

Barnes, J. E., & Hernquist, L. 1992, Nature, 360, 715

Barnes, J. E., & Hernquist, L. 1996, ApJ, 471, 115

Bekki, K., & Couch, W. J. 2001, ApJ, 557, L19

Bernlöhr, K. 1993, A&A, 270, 20

Biretta, J. A., et al. 2000, WFPC2 Instrument Handbook, Version 5.0, (Baltimore: STScI)

Borne, K. D., Bushouse, H., Lucas, R. A., & Colina, L. 2000, ApJ, 529, 77

Bryant, P. M., & Scoville, N. Z. 1999, AJ, 117, 2632

Bushouse, H. A., & Stanford, S. A. 1992, ApJS, 79, 213

Bushouse, H. A., & Werner, M. W. 1990, ApJ, 359, 72

Carollo, C. M., Franx, M., Illingworth, G. D., & Forbes, D. A. 1997, ApJ, 481, 710

Carral, P., Turner, J. L., & Ho, P. T. P. 1990, ApJ, 362, 434

Dahari, O. 1985, ApJS, 57, 643

Dubinski, J., Mihos, J. C., & Hernquist, L. 1996, ApJ, 462, 576

Duc, P. A., & Brinks, E. 2001, in ASP Conf. Proc. 240, Gas and Galaxy Evolution, ed. J. E. Hibbard, M. Rupen, & J. H. van Gorkom (San Francisco: ASP), 181

Elmegreen, B. G., Kaufman, M., & Thomasson, M. 1993, ApJ, 412, 90

English, J., Norris, R. P., Freeman, K. C., & Booth, R. S. 2003, AJ, 125, 1134

Fabbiano, G., Schweizer, F., & Mackie, G. 1997, ApJ, 478, 542

Ford, H. C., Illingworth, G. D., Clampin, M., Hartig, G., the ACS Science Team and ESA 2002, preprint (STScI-PRC02-11d)

Georgakakis, A., Forbes, D.A., & Norris, R.P. 2000, MNRAS, 318, 124

Hattori, T., Yoshida, M., Ohtani, H., Ishigaki, T., Sugai, H., Hayashi, T., Ozaki, S., & Ishii, M. 2002, PASJ, 54, 393

Hernquist, L. 1992, ApJ, 400, 460

Hernquist, L., & Mihos, J. C. 1995, ApJ, 448, 41

Hibbard, J. E., & Mihos, J. C. 1995, AJ, 110, 140

Hibbard, J. E., & van Gorkom, J. H. 1996, AJ, 111, 655

Hibbard, J. E., Guhathakurta, P., van Gorkom, J. H, & Schweizer, F. 1994, AJ, 107, 67

Hibbard, J. E., van der Hulst, J. M., Barnes, J. E., & Rich, R. M. 2001, AJ, 122, 2969

Hibbard, J. E., & Yun, M. S. 1999, ApJ, 522, L93

Holtzman, J. A., Burrows, C. J., Casertano, S., Hester, J. J., Trauger, J. T., Watson, A. M., & Worthey, G. 1995, PASP, 107, 1065

Hutchings, J. B., & Neff, S. G. 1992, AJ, 104, 11

Joseph, R. D., & Wright, G. S. 1985, MNRAS, 214, 87

Joy, M., & Harvey, P.M. 1987, ApJ, 315, 480

Keel, W. C., Kennicutt, R. C., Jr., Hummel, E., & van der Hulst, J. M. 1985, AJ, 90, 708

Kewley, L. J., Heisler, C. A., Dopita, M. A., & Lumsden, S. 2001, ApJS, 132, 37

Kotilainen, J. K., Moorwood, A. F. M., Ward, M. J., & Forbes, D. A. 1996, A&A, 305, 107

Kotilainen, J. K., Reunanen, J., Laine, S., & Ryder, S. D. 2001, A&A, 366, 439

Landini, M., Natta, A., Oliva, E., Salinari, P., & Moorwood, A. F. M. 1984, A&A, 134, 284

Lipari, S., Díaz, R., Taniguchi, Y., Terlevich, R., Dottori, H., & Carranza, G. 2000, AJ, 120, 645

Lira, P., Ward, M. J., Zezas, A., Alonso-Herrero, A., & Ueno, S. 2002, MNRAS, 330, 259

Lonsdale, C. J., Persson, S. E., & Matthews, K. 1984, ApJ, 287, 95

Mengel, S., Lehnert, M. D., Thatte, N., Tacconi-Garman, L. E., & Genzel, R. 2001, ApJ, 550, 280

Mihos, J. C., & Hernquist, L. 1994a, ApJ, 431, L9

Mihos, J. C., & Hernquist, L. 1994b, ApJ, 438, L47

Mihos, J. C., & Hernquist, L. 1996, ApJ, 464, 641

Mihos, J. C., Bothun, G. D., & Richstone, D. O. 1993, ApJ, 418, 82

Mihos, J. C., McGaugh S. S., & de Blok, W. J. G. 1997, ApJ, 477, L49

Mihos, J. C., Dubinski, J., & Hernquist, L. 1998, ApJ, 494, 183

Miller, B. W., Whitmore, B. C., Schweizer, F., & Fall, S. M. 1997, AJ, 114, 2381

Milosavljević, M., & Merritt, D. 2001, ApJ, 563, 34

Neff, S. G., & Ulvestad, J. S. 2000, AJ, 120, 670

Noguchi, M. 1988, A&A, 201, 37

Norris, R. P., & Forbes, D. A. 1995, ApJ, 446, 594

Quinlan, G. D., Hernquist, L., & Sigurdsson, S. 1995, ApJ, 440, 554

Quinlan, G. D., & Hernquist, L. 1997, New Astron., 2, 533

Rafanelli, P., & Marziani, P. 1992, AJ, 103, 743

Read, A. M., & Ponman, T. J. 1998, MNRAS, 297, 143

Ridgway, S. G., Wynn-Williams, C. G., & Becklin, E. E. 1994, ApJ, 428, 609

Sanders, D. B., Soifer, B. T., Elias, J. H., Madore, B. F., Matthews, K., Neugebauer, G., & Scoville, N. Z. 1988a, ApJ, 325, 74

Sanders, D. B., Scoville, N. Z., Sargent, A. I., & Soifer, B. T. 1988b, ApJ, 324, L55

Schweizer, F. 1982, ApJ, 252, 455

Schweizer, F. 1990, in "Dynamics and Interactions of Galaxies", ed. R. Wielen (Heidelberg: Springer), 60

Schweizer, F. 1996, AJ, 111, 109

Schweizer, F. 1998, in "Galaxies: Interactions and Induced Star Formation", Saas-Fee Advanced Course 26, ed. D. Friedli, L. Martinet, & D. Pfenniger, (Berlin: Springer–Verlag), 105

Schweizer, F., Miller, B. W., Whitmore, B. C., & Fall, S. M. 1996, AJ, 112, 1839

Scoville, N. Z., et al. 2000, AJ, 119, 991

Springel, V., & White, S. D. M. 1999, MNRAS, 307, 162

Stanford, S. A., & Balcells, M. 1990, ApJ, 355, 59

Stanford, S. A., & Balcells, M. 1991, ApJ, 370, 118

Stanford, S. A., & Bushouse, H. A. 1991, ApJ, 371, 92

Stauffer, J. R. 1982a, ApJ, 262, 66

Stauffer, J. R. 1982b, ApJS, 50, 517

Surace, J. A., Sanders, D. B., & Evans, A. S. 2001, AJ, 122, 2791

Toomre, A. 1977, in "The Evolution of Galaxies and Stellar Populations," ed. B. M. Tinsley & R. B. Larson (New Haven: Yale Univ.), 401

Toomre, A., & Toomre, J. 1972, ApJ, 178, 623

Vacci, L., Alonso-Herrero, A., & Rieke, G. H. 1998, ApJ, 504, 93

van der Marel, R. P., & Zurek, D. 2000, in ASP Conf. Ser. 197, "Dynamics of Galaxies: from the Early Universe to the Present", Ed. F. Combes, G. A. Mamon, & V. Charmandaris, 323

Veilleux, S., Kim, D.-C., Sanders, D. B., Mazzarella, J. M., & Soifer, B. T. 1995, ApJS, 98, 171

Verdoes Kleijn, G. A., Baum, S. A., de Zeeuw, P. T., & O'Dea, C. P. 1999, AJ, 118, 2592

Véron–Cetty, M.–P., & Véron, P. 1986, A&A, 66, 335

Wang, Z., Schweizer, F., & Scoville, N. Z. 1992, ApJ, 396, 510

Weedman, D. 1983, ApJ, 243, 756

Whitmore, B. C., & Schweizer, F. 1995, AJ, 109, 960

Whitmore, B. C., Miller, B. W., Schweizer, F., & Fall, S. M. 1997, AJ, 114, 1797

Whitmore, B. C., Zhang, Q., Leitherer, C., Fall, S. M., Schweizer, F., & Miller, B. W. 1999, AJ, 118, 1551

Young, P. J. 1980, ApJ, 242, 1232

Yun, M. S., & Hibbard, J. E. 2001, ApJ, 550, 104

Zepf, S. E., Ashman, K. M., English, J., Freeman, K. C., & Sharples, R. M. 1999, AJ, 118, 752

Zezas, A., Fabbiano, G., Rots, A. H., & Murray, S. S. 2002a, ApJ, 577, 710

Zezas, A., Fabbiano, G., Rots, A. H., & Murray, S. S. 2002b, ApJS, 142, 239

Zhang, Q., Fall, S. M., & Whitmore, B. C. 2001, ApJ, 561, 727

Zwicky, F. 1950, Experentia, 6, 441

Zwicky, F. 1956, Ergebnisse der Exacten Naturwissenschaften, 29, 344

Zwicky, F. 1964, ApJ, 140, 1467